PHILOSOPHICAL TRANSACTIONS OF THE ROYAL SOCIETY A MATHEMATICAL, PHYSICAL & ENGINEERING SCIENCES

Free and Mixed Convective Flow of Air in a Heated Cavity of Variable rectangular Cross Section and Orientation

K. S. Chen, J. A. C. Humphrey and F. S. Sherman

Phil. Trans. R. Soc. Lond. A 1985 **316**, 57-84
doi: 10.1098/rsta.1985.0056

Phil. Trans. R. Soc. Lond. A **316**, 57–84 (1985) [57]
Printed in Great Britain

FREE AND MIXED CONVECTIVE FLOW OF AIR IN A HEATED CAVITY OF VARIABLE RECTANGULAR CROSS SECTION AND ORIENTATION

By K. S. CHEN, J. A. C. HUMPHREY and F. S. SHERMAN
Mechanical Engineering Department, University of California, Berkeley, Berkeley, California 94720, *U.S.A.*

(*Communicated by D. B. Spalding, F.R.S. – Received* 30 *January* 1985)

[Plates 1–4]

CONTENTS

Free and mixed convection in a strongly heated cavity of rectangular cross section have been investigated experimentally, to observe the effects of cavity shape and inclination and of ambient wind on the velocity and temperature distributions. The long edges ($c = 0.533$ m) of the cavity were horizontal and parallel to an axis around which the cavity could be rotated. The aperture plane was either vertical ($\alpha = 0°$), or inclined facing downward at $\alpha = 20°$ or $\alpha = 45°$. The height of the aperture, b, was always 0.0947 m, while the depth of the cavity, a, was set so that $a/b = 0.5$, 1.0, or 1.46. The bottom and back walls were electrically heated but the top wall was indirectly heated by conduction and radiation. The absolute average temperature of the wall, T_c, was 2.21 times the absolute temperature at infinity, T_∞, and the Grashof number based on the difference of these two temperatures, with physical properties evaluated at T_∞, was 4.2×10^7. The Prandtl number was that of air, $Pr \approx 0.7$.

In the studies of mixed convection, the axis of rotation was horizontal and normal to the ambient wind, U_∞. When the aperture faced directly upstream the inclination angle was $\alpha = 0°$. The Reynolds number, $Re = bU_\infty/\nu_\infty$, was varied from $Re = 120$–1100, where free convection was dominant, to $Re = 2000$–8740, where forced convection was dominant.

For both free and mixed convection, wall and gas temperatures were measured with thermocouples and shadowgraph pictures were taken. For pure free convection, three time-averaged velocity components, the corresponding normal Reynolds stress components and one off-diagonal Reynolds stress component were measured by using a two-colour laser–Doppler velocimeter with the assistance of a minicomputer for automated data collection and reduction.

The experiments were largely exploratory and revealed a wealth of interesting phenomena. These include instabilities that have previously been seen in more simply bounded flows and periodic oscillations that seem unique to the open cavity.

This application of laser–Doppler velocimetry is interesting in its own right, confronting large variations in index of refraction, extraordinarily high percentage fluctuations in velocity and density and great difficulty in assuring the uniform distribution of light-scattering particles.

1. Introduction

Free convection in and around very hot cavities, with or without an ambient wind, has become important in connection with central solar energy receivers, the control of compartment fires and combustion in furnaces. The study of heated cavity flow phenomena is scientifically rewarding, because a single flowfield may contain regions in which the force of gravity is hydrodynamically destabilizing, quite close to other regions in which the same force is stabilizing. Thus convective plumes and internal waves may appear side by side and may interact in interesting ways.

The superposition of an ambient wind, particularly when its inertia competes more or less directly with the buoyancy forces that drive free convection, introduces other fascinating phenomena. Sometimes even a very faint breeze may cause a surprisingly large effect, presumably when the free convection flow is close to the threshold of some instability.

When the solid boundaries of the flow are very hot, the dimensionless overheat $\Delta T/T_\infty$ must take its place as an independently important parameter, in addition to being a factor in the Grashof number. The independent effects that we associate with $\Delta T/T_\infty$ itself are variability of the density, ρ, as an indicator of inertia; variability of the viscosity, μ, and of the thermal conductivity, k; and the direct kinematic effect of thermal expansion. These effects are all absent from the Boussinesq approximation, which has been used in most theory and data correlations up to the present time.

PHILOSOPHICAL TRANSACTIONS OF THE ROYAL SOCIETY A MATHEMATICAL, PHYSICAL & ENGINEERING SCIENCES

Unlike the shock waves that appear when the Mach number increases, or the instabilities that appear when the Grashof or Reynolds numbers increase, the phenomena accompanying increases in $\Delta T/T_\infty$ do not seem to be qualitatively remarkable. Thus it is challenging to try to identify the independent effects of this parameter, or to attempt to postpone the need to recognize it as independently important by evaluating the temperature-dependent properties in the other parameters at cleverly chosen average temperatures.

The present study was undertaken because of the need to understand the influence of configuration shape and orientation on the free and mixed convection flow in strongly heated cavities. In an effort to complement similarly motivated, large-scale, three-dimensional investigations (discussed below), our efforts have focused on elucidating fundamental phenomena in somewhat simplified circumstances. Thus, in this study, the shape and orientation of the cavity (shown schematically in figure 1) are designed to encourage a flow that is primarily two-dimensional in a time-averaged sense and to provide surroundings that are either quiescent or in steady uniform motion, while the overheat ratio is allowed to be large enough to be independently important.

1.1. *Related investigations*

In contrast to forced convection, free and mixed convection in cavity configurations have received sparse attention. Detailed literature reviews are given in Humphrey *et al.* (1980, 1983). We summarize here some of the results of the studies most relevant to the present work.

Eyler (1980), Le Quere *et al.* (1981) and Penot (1982) have performed numerical calculations of two-dimensional buoyancy-driven laminar flow in heated cavities of rectangular cross section. The procedure of Le Quere *et al.* (1981), unlike the other two, was not subject to the Boussinesq approximation. In that study, the cavity aspect ratio and inclination angle were varied to investigate their respective influence on the flow. The calculations revealed low-frequency flow oscillations when a critical Grashof number was exceeded and a marked reduction in the convective losses when the cavity was tilted forward so that the aperture plane faced downwards. By using the experimental system described here, Chen *et al.* (1983) confirmed the presence of flow oscillations in heated rectangular cavities. Highly structured and predominantly two-dimensional, these eddies appeared with a periodicity of 1–2 Hz and were observed in cavities with $a/b = 0.5$ and 1, when $\alpha = 20°$ and 0° respectively and when $0.31 \leqslant \Delta T/T_\infty \leqslant 0.44$ (see figure 1 for notation). These conditions correspond to $Gr \approx 9.6 \times 10^6$, which is close to the critical value of $Gr \approx 10^7$ reported by Le Quere *et al.* (1981). Chen *et al.* (1983) also show preliminary flow-visualization results for the effect of increasing α from 0° to 45° on the free convection flow in a cavity with $a/b = 1$ and $\Delta T/T_\infty \approx 1.37$. For these conditions, $Gr \approx 3.9 \times 10^7$ and the high value of $\Delta T/T_\infty$ ensured that when $\alpha = 0°$ the flow was turbulent. The authors observed that increasing α reduced the level of turbulent activity in the cavity because of two effects: (i) damping of turbulent fluctuations by the stable stratification of hot air trapped in the cavity and (ii) reduction in the intensity and magnitude of the recirculating flow region arising along the bottom wall of the cavity. The low-frequency oscillations were not discernible in the turbulent flow régime.

By using a laser–Doppler velocimeter (l.D.v.), Sernas & Kyriakides (1982) have obtained limited measurements of the velocity components parallel to the back and top walls of a two-dimensional cavity with $a/b = 1$, $\alpha = 0°$ and $Gr = 10^7$. The overheat ratio was fairly small and only the back and top walls were heated, the bottom wall being kept at room temperature.

As a result the flow was entirely in the laminar régime and displayed none of the striking characteristics observed by Chen *et al.* (1983).

Free convection heat transfer in cubical cavities has been investigated by Hess & Henze (1984), Penot (1981), Mirenayat (1981) and Kraabel (1983). By using water as the working fluid, Hess & Henze (1984) were able to obtain values of the Rayleigh number ($Ra = Gr \times Pr$) ranging from 2×10^{10}–2×10^{11} at relatively low values of $\Delta T/T_\infty$. Only the back wall of their cube was heated, which ensured a streamlined flow up to $Ra = 7 \times 10^{10}$–9×10^{10} when the flow became turbulent. The effects on fluid motion and heat transfer of constricting the flow entering and leaving the cavity were investigated. In the other three studies the working fluid was air.

In consecutive investigations, Penot (1981) and Mirenayat (1981) studied the flow in their cavity by using smoke and the l.D.v. technique. In these experiments, the five walls of the cavity were held at uniform, constant, equal temperature. Although the measurements of velocity are sparse (and of questionable reliability), Mirenayat (1981) also obtained extensive measurements of heat transfer as a function of α and Gr for $0.04 \leqslant \Delta T/T_\infty \leqslant 0.47$. The author defined an overall heat transfer coefficient as $h = \dot{Q}/5L^2\Delta T$, where $5L^2$ is the total heated area with heat flow $\dot{Q}$ induced by the temperature different $\Delta T = T_c - T_\infty$. The Nusselt number was then defined as $Nu = hL/k_\infty$, and a correlation was reported in the form

$$Nu = mGr^n \quad (10^7 < Gr < 4 \times 10^9), \tag{1.1}$$

with the Grashof number defined as $Gr = g(T_c - T_\infty)\, L^3/T_\infty \nu_\infty^2$. Here, m and n denote parameters that depend on the cavity inclination angle α. Typically, $0.03 \leqslant m \leqslant 0.12$ and $0.30 \leqslant n \leqslant 0.37$, strongly supporting the $\frac{1}{3}$ power dependence of Gr proposed by Mirenayat (1981) for the range of Gr investigated.

The large characteristic dimension (2.2 m) of the cavity investigated by Kraabel (1983) permitted obtaining values of Grashof number as large as 1.2×10^{12} for overheat ratios ranging between $\Delta T/T_\infty = 0.39$ and 2.55 approximately. In these experiments, the five walls of the cavity were held at uniform, constant, equal heat flux. Air temperature, velocity, enthalpy flux and radiative heat-flux distributions were determined on the aperture plane. From these data, convective (and radiative) heat losses were accurately determined and, by using the above definitions of Nu and Gr, the following correlation was reported:

$$Nu = 0.088\, Gr^{\frac{1}{3}} (T_c/T_\infty)^{0.18} \quad (10^7 < Gr < 1.2 \times 10^{12}). \tag{1.2}$$

This result is for the inclination angle $\alpha = 0°$, the only case tested, and it agrees well with that of Mirenayat (1981), who found $m = 0.093$ and $n = 0.33$ for $\alpha = 0°$. Both sets of data imply, because $Gr^{\frac{1}{3}}$ is linearly proportional to L, that the average heat-transfer coefficient is independent of cavity size.

The above investigations were all performed for purely free convection flow and have added little to an improved understanding of the fluid mechanics in cavities. In addition, no relevant work was found in the literature pertaining to the mixed convection régime. However, because the elemental component of the heated cavity configuration is the flat plate, it seems reasonable to expect that some of the features of heated cavity flows will be similar to (or a result of, some of those associated with the heated flat plate configuration. The same logic leads us to expect similarities between the flows in cavities and the flows in enclosures (sealed cavities). A detailed review of several experimental and theoretical investigations dealing with flat plate and enclosure configurations that were especially meaningful to this work and have contributed to

our understanding is given in Humphrey *et al.* (1983). Of these studies, the findings of Rotem & Claassen (1969) and Pera & Gebhart (1973) pertaining to unstable free convection flow over horizontal (or nearly horizontal) flat plates with upward-facing heated surfaces, and the inclined flat plate instability studies by Lloyd & Sparrow (1970), Pera & Gebhart (1973) and Chen & Tszoo (1982) have strongly influenced the interpretation of some of our own findings.

1.2. *Analytical approximations applicable to this work*

Although this is a report of laboratory measurements, the interpretation of some of the data requires justification of underlying theoretical approximations. This has been given elsewhere (Le Quere *et al.* 1981; Humphrey *et al.* 1983) and is summarized here.

The main point to establish is that, under the conditions of our experiment, we can neglect the terms on the right-hand side of the energy equation

$$\nabla\cdot(\rho h\boldsymbol{u}+\boldsymbol{q}) = -\partial/\partial t(\rho h)+\mathrm{D}p/\mathrm{D}t+\Phi. \tag{1.3}$$

In this equation, h is enthalpy, $\boldsymbol{u}$ the velocity vector, $\boldsymbol{q}$ the conductive heat-flux vector, p is pressure, Φ is the viscous dissipation function and t is time.

The arguments rely on invoking the perfect-gas relation $\rho h = \gamma p/(\gamma-1)$, where the ratio of specific heats, γ, is assumed constant. Then (1.3), which is exact, can be reformulated as

$$(\gamma/\gamma-1)\,p(\nabla\cdot\boldsymbol{u})+(\nabla\cdot\boldsymbol{q}) = -(1/\gamma-1)\,\mathrm{D}p/\mathrm{D}t+\Phi, \tag{1.4}$$

which is exact for a perfect gas. Conservative estimates show that p, as a coefficient of $\nabla\cdot\boldsymbol{u}$, can be approximated by the constant atmospheric pressure, p_∞. It can also be shown that the dissipation and material derivative terms are both negligibly small relative to $\nabla\cdot\boldsymbol{q}$. Thus, (1.4) is accurately approximated by

$$(\gamma/\gamma-1)\,p_\infty(\nabla\cdot\boldsymbol{u})+(\nabla\cdot\boldsymbol{q}) = 0. \tag{1.5}$$

The qualitative implication of (1.5) is that we should not expect to see new flow features, such as shock waves or acoustic resonances, simply because $\Delta T/T_\infty > 1$. Where the conductive heat flux converges, thermal expansion causes simultaneous divergence of the velocity field. Elsewhere the velocity field is solenoidal.

1.3. *Outline of the paper*

A brief description of experimental equipment and procedures is given in §2. Complete details are available in Humphrey *et al.* (1983). In §3 we describe and discuss our observations, first for free convection, then for mixed convection. Some brief comments on experimental uncertainties are presented in §4, mostly to stimulate an appreciation for the difficulty associated with laser–Doppler velocimetry under present conditions and to encourage further work to reduce these difficulties. Again, a much more detailed analysis is presented by Humphrey *et al.* (1983).

2. Experimental equipment and procedure

2.1. *The heated cavity*

Figure 1 shows the dimensions of the cavity and the coordinate system used for the presentation of velocity and temperature profiles.

The cavity is formed by three thick copper slabs and two borosilicate glass end-plates. The

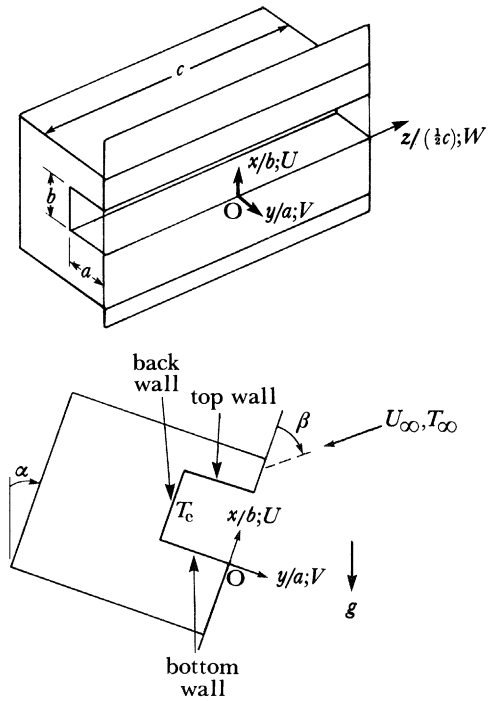

FIGURE 1. Perspective (top) and side (bottom) views of the cavity test section. Dimensions: $a = 0$–147.67 mm, $b = 94.66$ mm, $c = 533.4$ mm; $0 \leqslant a/b \leqslant 1.56$; $c/b = 5.63$. In this study the direction of U_∞ was always normal to the gravity vector ($\beta = 90 - \alpha$).

sixth face, called the aperture plane, is open. The copper slabs were backed with Fiberfrax Duraboard insulation and bolted to an aluminium frame.

The position of the back wall and hence the depth of the cavity could be adjusted. The tests reported here employed three depth ratios, $a/b = 0.5$, 1.0 and 1.46. The whole assembly was supported on a steel frame, about 1.5 m above the floor. The long axis of the cavity (z axis) was horizontal and the cavity could be rotated around that axis. Tests were run with the aperture plane vertical ($\alpha = 0°$), or inclined facing down at $\alpha = 20°$ or 45°. In tests of mixed convection, the ambient wind was horizontal and normal to the long axis of the cavity.

The bottom and back walls were heated electrically, and the top wall was heated by conduction from the back wall and by radiation from both the electrically heated walls. Several thermocouples embedded near the inner surface of each wall provided the data on cavity surface temperatures and the input for a temperature controller. The great thermal capacity and thermal conductivity of the copper walls allowed us to maintain constant and uniform wall temperatures.

The nominal wall temperatures for almost all our observations were

$$T_{\text{bottom}} = 673 \text{ K}, \quad T_{\text{back}} = 673 \text{ K}, \quad T_{\text{top}} = 611 \text{ K}.$$

The top and bottom walls were usually a few degrees warmer where they were in contact with the back wall, but most of the temperature jump from wall to wall occurred across an air gap and copper oxide layer. Because of the thermocouple locations, the spanwise uniformity of wall temperature could only be judged directly when $a/b = 1.46$; then variations of ± 1 K around the mean were observed.

2.2. *Air temperature measurements in the cavity aperture plane*

Twelve chromel–alumel thermocouple wires of diameter 0.003 in (76 μm) were used to measure the temperature of the air in the cavity aperture plane. The thermocouple wires were spring-mounted to accommodate thermal expansion; the junctions could be positioned at predetermined locations with uncertainties of ± 0.25 mm in x and y, ± 5 mm in z. Thermal expansion of the cavity adds some systematic uncertainty to the location of the junctions relative to the heated cavity, but this would have no significant effect on the observations reported here.

Voltages from these thermocouples were sampled once per second, 50 or 100 times per observation point. Means and standard deviations of these samples were calculated. Because of the substantial heat capacity of the wires and the periodic sampling procedure, these standard deviations may underestimate the corresponding measures of true air temperature fluctuations by a factor as large as two. A detailed analysis is provided by Chen (1983).

2.3. *Wind tunnel and wind speed measurement*

For observations of mixed convection, the cavity was installed in the plenum chamber of a low-speed, low-turbulence wind tunnel. The chamber cross section is 3.05 m × 3.05 m; the cavity obstructed about 2.8% of this area. The plenum chamber is followed by a 14:1 contraction section; the velocity in the plenum chamber was determined from the pressure drop across the contraction, the Bernoulli equation and the continuity equation for one-dimensional flow. This method was satisfactorily checked against local measurements of the rate of vortex shedding from cylinders in the plenum chamber.

The available speed range was $0.09 < U_\infty < 1.4$ ms^{-1}; the estimated turbulence level (scaled up by a factor of 14^2 from values measured in the test section) was

$$(\overline{u'^2})^{\frac{1}{2}}/U_\infty \approx 0.04.$$

2.4. *Flow visualization*

Because the flow-visualization studies were intended to be exploratory and largely qualitative, a simple shadowgraph method was used. A simple light source (either a 1000 W argon–xenon lamp or a 300 W Kodak slide-projector lamp) produced a roughly collimated light beam, the axis of which coincided approximately with the z-axis of our coordinate system. When periodic pulsation appeared in the flow, stroboscopic illumination was used to freeze various phases of the motion and to determine oscillation frequencies.

Some movies were taken at 32 frames s^{-1}; the pictures presented here are snapshots, taken at 0.001 s exposure in most cases.

2.5. *Laser–Doppler velocimeter system*

The free convection flows were seeded with tiny vegetable oil droplets. These scattered blue (448 nm) and green (514.5 nm) light when they crossed a probe volume formed by intersecting the laser beams, arranged to allow simultaneous measurement of two orthogonal components of the droplet velocity. The probe volume dimensions were approximately 0.137 mm × 0.137 mm × 3.8 mm.

We employed a DISA 55X Modular Series l.D.v., with frequency shifting, in the backscatter mode; the light source was a 2 W Lexel argon-ion laser.

The location of the probe volume was controlled and the signals from the photomultiplier tubes were analysed by a PDP 11/34 minicomputer, which also controlled the operation of two DISA 55L96 Doppler signal processors. The probe volume could be displayed along any of the coordinate axes by stepping motors operated by the minicomputer.

The many details of this system and its operation, which are relevant to an assessment of the accuracy and interpretation of the l.D.v. data, are given in Humphrey *et al.* (1983). We only note here that:

(i) only one droplet scattered light from the probe volume at any given time;

(ii) the computer recovery time was short compared with the time between Doppler bursts;

(iii) the rate of validated simultaneous measurements of two velocity components in the cavity aperture plane was 50 Hz or less (the non-coincident data rate being somewhat higher);

(iv) at locations well inside the cavity, the data rate for validated simultaneous measurements of two velocity components was so low that only a single component was measured;

(v) samples of 1000 measurements were used for statistical analysis of the two-component data; 500 were used for one-component data;

(vi) the precision of the probe volume location was about ± 0.3 mm.

The vegetable oil droplets, from 0.2–2 μm in diameter, were generated by a pressure-regulated blast atomizer of the type described by Drain (1980). The droplets were blown upward in a jet that entrained, at first vigorously and later very gently, surrounding air into which the droplets were mixed. After this initial mixing process, in which there must have been substantial motion of droplets through the surrounding air, the seeded air became part of the updraft induced by the hot cavity. In this relatively steady and uniform induced flow, and even in the flow within the cavity itself, the droplets must have moved with very nearly the local instantaneous velocity of the air.

2.6. *Experimental conditions and procedure*

The nominal ambient temperature for all the experiments was $T_\infty = 295$ K. An average cavity temperature

$$T_c = \tfrac{1}{3}(T_{\text{bottom}} + T_{\text{back}} + T_{\text{top}}) = 652 \text{ K},$$

was used in the dimensionless parameters

$$\Delta T/T_\infty = (T_c - T_\infty)/T_\infty = 1.21,$$

and

$$Gr = (g\Delta T b^3)/(T_\infty \nu_\infty^2) = 4.2 \times 10^7.$$

Run-to-run variations in these parameters were less than $\pm 4\%$ of the nominal values.

For observations of free convection, special precautions were taken to ensure a quiescent, thermally unstratified environment. Thus the test stand was centred inside a canvas windshield that formed a vertical prism of 1.5 m × 1.5 m cross section, extending from the top of the stand to within 0.3 m of the floor. The prism allowed ample clearance in front of the cavity, so that interference with the steady induced flow was negligible. Residual disturbances of the free convection flow seemed to be a result of unsteady separation of the induced flow, from sharp edges at the bottom of the apparatus and at the bottom aperture edge.

Before an experimental run, the cavity inclination angle and aspect ratio were set to the desired values. The cavity was brushed clean of copper oxide scale formed from previous runs.

Power was then applied to the strip heaters until steady-state conditions had been achieved, as indicated by the measurements of temperature at the cavity walls. This warm-up period lasted about $2\frac{1}{2}$–3 h.

For the studies in the wind tunnel, changes in wind speed had little effect on the surface temperatures of the cavity, the gas temperatures responded swiftly to changes in wind speed and the photographs and temperature data could be taken as soon as the new wind speed was stabilized and measured. Each of the twelve aperture-plane thermocouples was read 100 times at one-second intervals, so the time for each run was approximately 25 min. Free convection runs in which l.D.v. data were gathered were much more time-consuming, typically lasting five hours. The long-term stability of the temperature-control system and, to a lesser degree, the constancy of ambient conditions, were obviously important. These long tests were ordinarily run at night.

Mean velocities and turbulent stresses were determined from formulae such as those shown below for U, $\overline{u'^2}$ and $\overline{u'v'}$,

$$U = \sum_{i=1}^{N} U_i \omega_i \Big/ \sum_{i=1}^{N} \omega_i, \tag{2.1}$$

$$\overline{u'^2} = \sum_{i=1}^{N} (U_i - U)^2 \omega_i \Big/ \sum_{i=1}^{N} \omega_i, \tag{2.2}$$

$$\overline{u'v'} = \sum_{i=1}^{N} (U_i - U)(V_i - V)\omega_i \Big/ \sum_{i=1}^{N} \omega_i. \tag{2.3}$$

In these formulae N is the number of instantaneous realizations. The quantity ω_i is the weight factor for the ith realization. If $\omega_i = 1$ the simple arithmetic mean is obtained; equal weight being given to each measurement.

Many authors, following McLaughlin & Tiederman (1973) have observed that equal weighting is inappropriate in principle, even for a uniformly seeded fluid, because fast-moving particles will traverse the optical probe volume more frequently than slow ones. Buchave *et al.* (1979) conclude from this that the proper weight factor is the duration of the signal returned from the ith scattering particle, Δt_i. Thus the time-averaging integral operation

$$U = \frac{1}{t}\int_{t_0}^{t_0+t} u(t')\,\mathrm{d}t' \tag{2.4}$$

is approximated by

$$U = \sum_{i=1}^{N} U_i \Delta t_i \Big/ \sum_{i=1}^{N} \Delta t_i. \tag{2.5}$$

The signals returned from fast particles are given smaller weights in the sum, in a way that compensates exactly for their abnormally frequent appearance.

Unfortunately, our data-acquisition computer system was not programmed to record the duration of each burst, and we could only estimate Δt_i from the measured values of U_i and V_i, the two velocity components normal to the axis of the optical probe volume. Because the probe volume is very slender, the axial component of particle speed has very little effect on the duration of the burst. Thus, when the two-component system was in use, we used the weight factor

$$\omega_i = (U_i^2 + V_i^2)^{-\frac{1}{2}}. \tag{2.6}$$

When the one-component system was in use, Δt_i might have been estimated from U_i; the speed of the fringes, V_f; the number of fringes crossed during the burst, N_f; and the distance between fringes, δ_f. Then,

$$\Delta t_i = N_f \delta_f / (V_f + U_i), \tag{2.7}$$

which would be an excellent estimate, except that our counter-logic imposed a maximum value on N_f of 255 and there was no provision for the recording of N_f.

Lacking any definitive estimates of particle residence time during the one-component measurements, we used two simple data-reduction schemes. The first was the simple equal-weight scheme for all signals, $\omega_i = 1$. The second assigned equal weight to all signals for which the measured velocity was less than 0.05 m s^{-1}, and a weight equal to $0.05/|U_i|$ for faster particles. Complete listings of both weighted and unweighted data are given in Humphrey *et al.* (1983).

3. Results and discussion

Table 1 shows the conditions investigated and the variables determined in this study. Conditions were limited to the three aspect ratios and three inclination angles listed. The table shows that in studies of mixed convection the parameter Gr/Re^2 was varied between 0.55 and 720 approximately.

3.1. *Free convection*

3.1.1. *Flow visualization*

Figure 2, plate 1, is a composition snapshot of typical free convection flows corresponding to the conditions listed in the caption. It is important to note that the cavity aperture-plane height, b, was the same for all experiments. Unequal photographic reductions give the false impression that this dimension varied.

We comment on these observations as follows.

(i) A strongly preheated boundary layer exists along the outer edge of the bottom heated plate.

(ii) This boundary layer separates at the sharp entry corner, when $\alpha = 0°$ and 20°, with a highly unsteady reattachment about halfway along the bottom wall when $a/b = 1.46$ and 1.0, and reattachment on the back wall, at $x/b \approx 0.25$, when $a/b = 0.5$. The size of the recirculation zone decreases as α is increased and the zone is barely visible when $\alpha = 45°$.

(iii) Plumes rise irregularly from the thermally unstable bottom boundary layer, starting at values of y/b that increased with increasing α. It is believed, from the experiments of Rotem & Claassen (1969), Lloyd & Sparrow (1970) and Pera & Gebhart (1973), and from the theoretical calculations of Chen & Tszoo (1982), that these plumes manifest the instability of bottom-heated boundary layers on nearly horizontal plates, to longitudinal vortex instabilities. No clear evidence of Tollmien–Schlichting (transverse wave) type instabilities was seen, nor was it to be expected, according to Chen & Tszoo (1982).

The theory of Chen & Tszoo (1982) predicts critical values of y, at which this instability is first possible for a given overall Grashof number. For our standard condition, $Gr = 4.2 \times 10^7$, the critical values of y/b are shown in the first column of table 2. The fourth column shows our estimates of the position, y/b, at which the plumes seemed clearly visible. Our values are, of course, much larger than those predicted to mark the onset of instability, because the disturbances grow fairly slowly. The dependence on α agrees qualitatively with the theory.

PHILOSOPHICAL TRANSACTIONS OF THE ROYAL SOCIETY A MATHEMATICAL, PHYSICAL & ENGINEERING SCIENCES

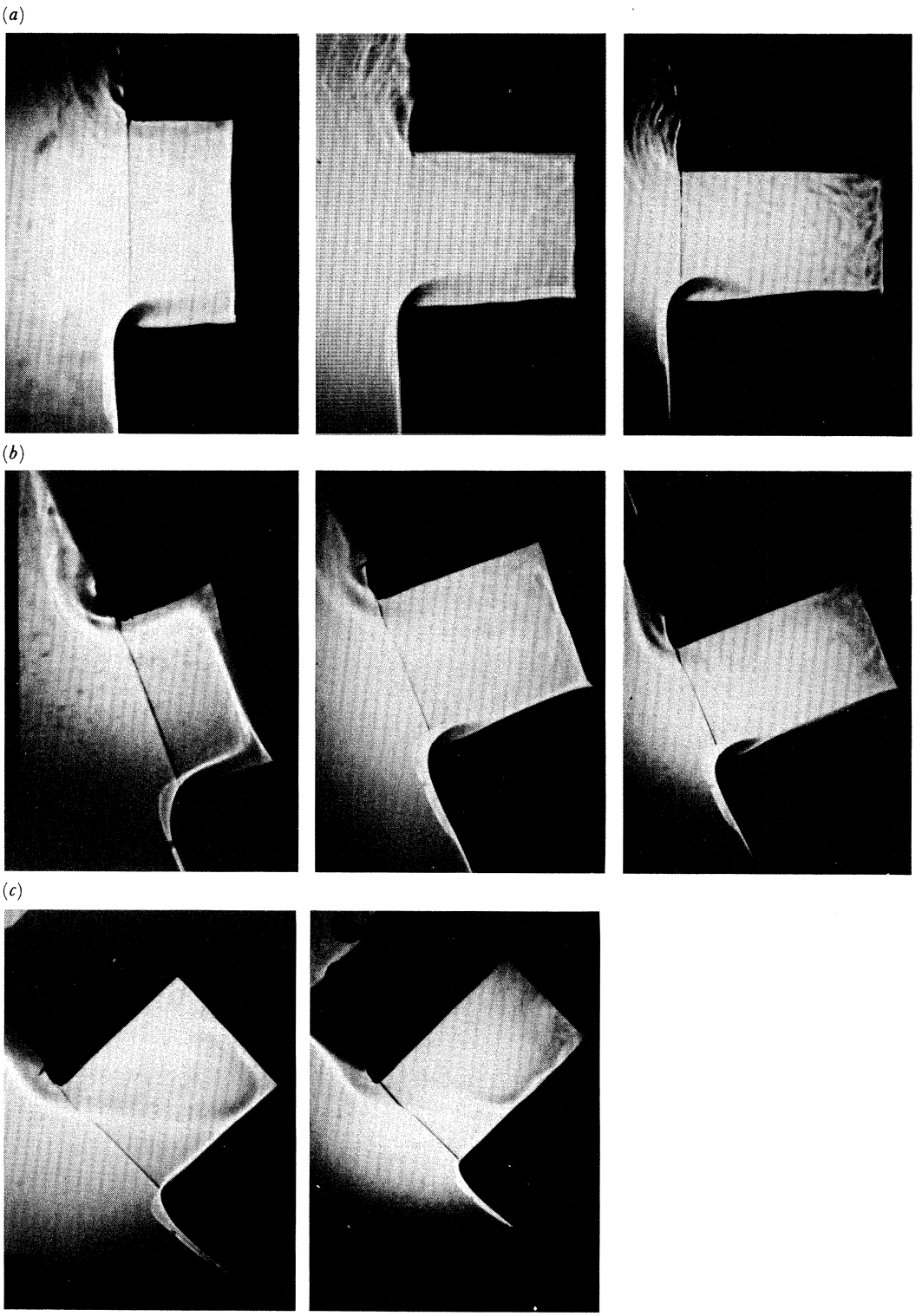

FIGURE 2. Shadowgraphs of the free-convection flow of air in rectangular cavities with $a/b = 0.5$, 1.0 and 1.46 (left to right) for three inclination angles of α: (*a*) 0°; (*b*) 20°; (*c*) 45°. Flow conditions: $\Delta T/T_\infty \approx 1.2$, $Gr \approx 4.2 \times 10^7$, $Pr \approx 0.7$. In all experiments the cavity aperture dimension, b, was the same. Unequal photographic reductions give the false impression that b varied.

(*Facing p.* 66)

PHILOSOPHICAL TRANSACTIONS OF THE ROYAL SOCIETY A MATHEMATICAL, PHYSICAL & ENGINEERING SCIENCES

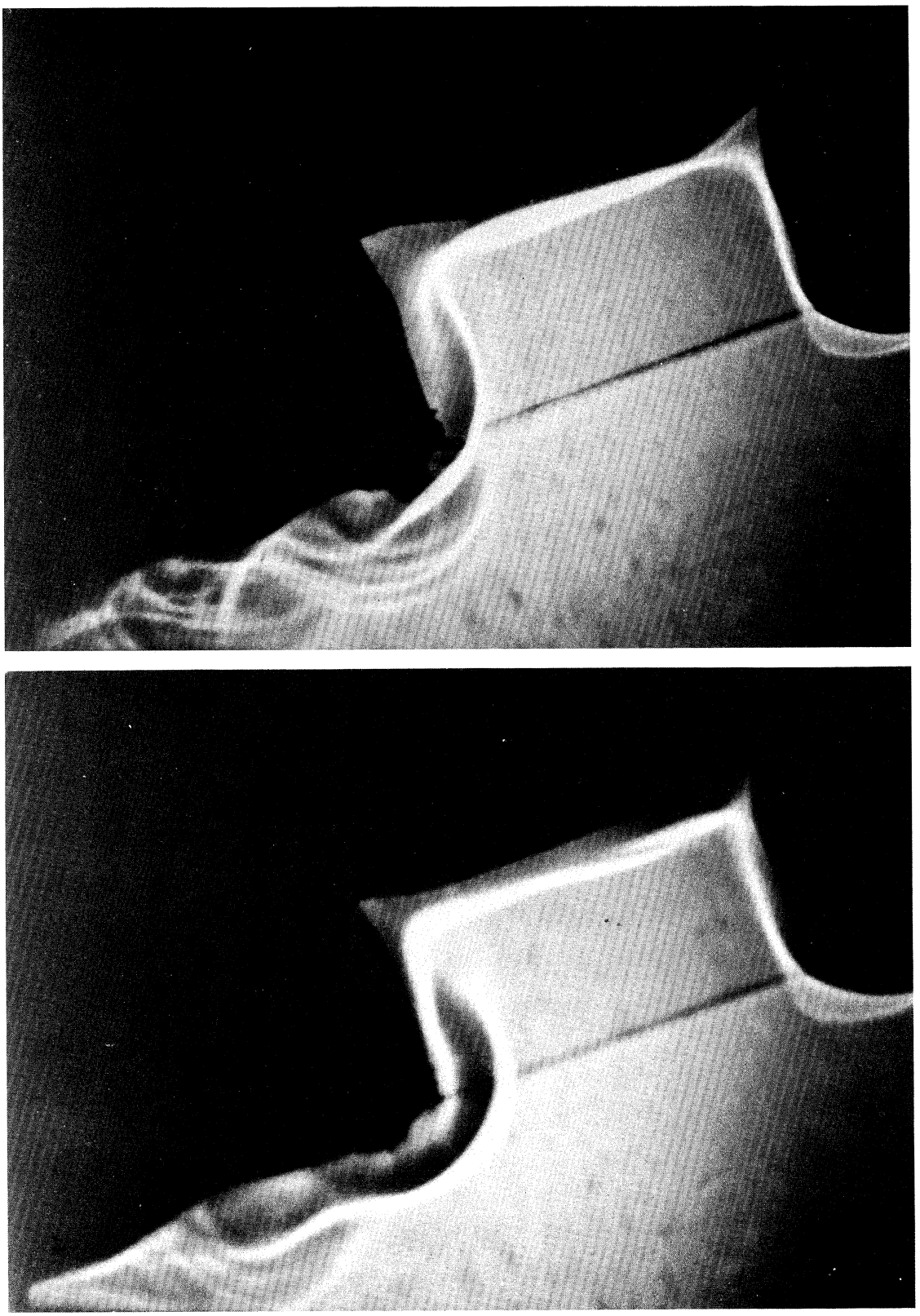

FIGURE 16. Large-scale, low-frequency organized cavity-flow oscillations frozen by stroboscopic pulsing of a point light source. Photographs are for different phases of a cycle.

PHILOSOPHICAL TRANSACTIONS OF THE ROYAL SOCIETY A MATHEMATICAL, PHYSICAL & ENGINEERING SCIENCES

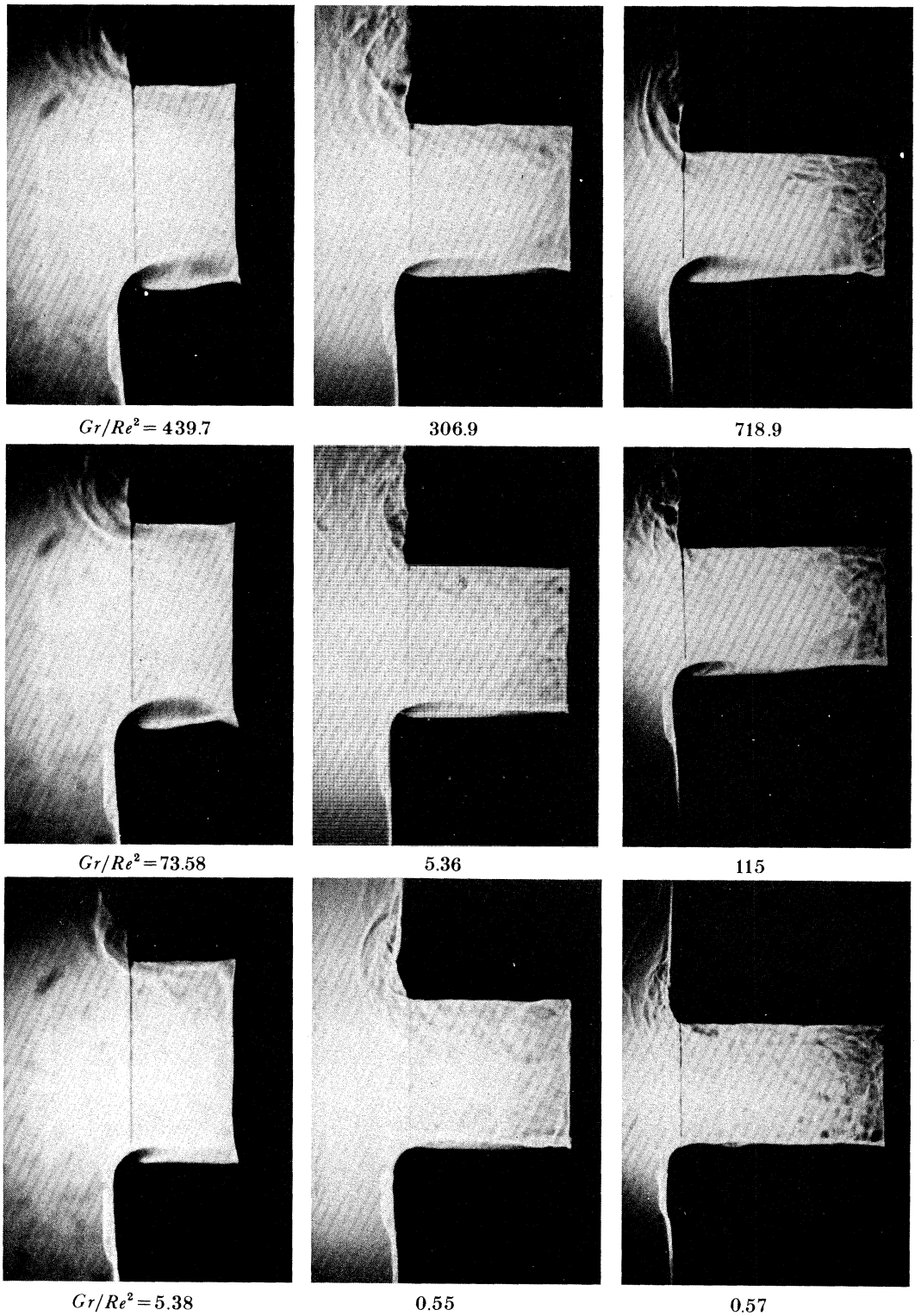

FIGURE 17. Shadowgraphs of heated-cavity flows with $\alpha = 0°$ and (from left to right) $a/b = 0.5$, 1.0 and 1.46 for different values of Gr/Re^2: $Gr \approx 4.1 \times 10^7$, $\Delta T/T_\infty \approx 1.2$ (average values).

PHILOSOPHICAL TRANSACTIONS OF THE ROYAL SOCIETY A MATHEMATICAL, PHYSICAL & ENGINEERING SCIENCES

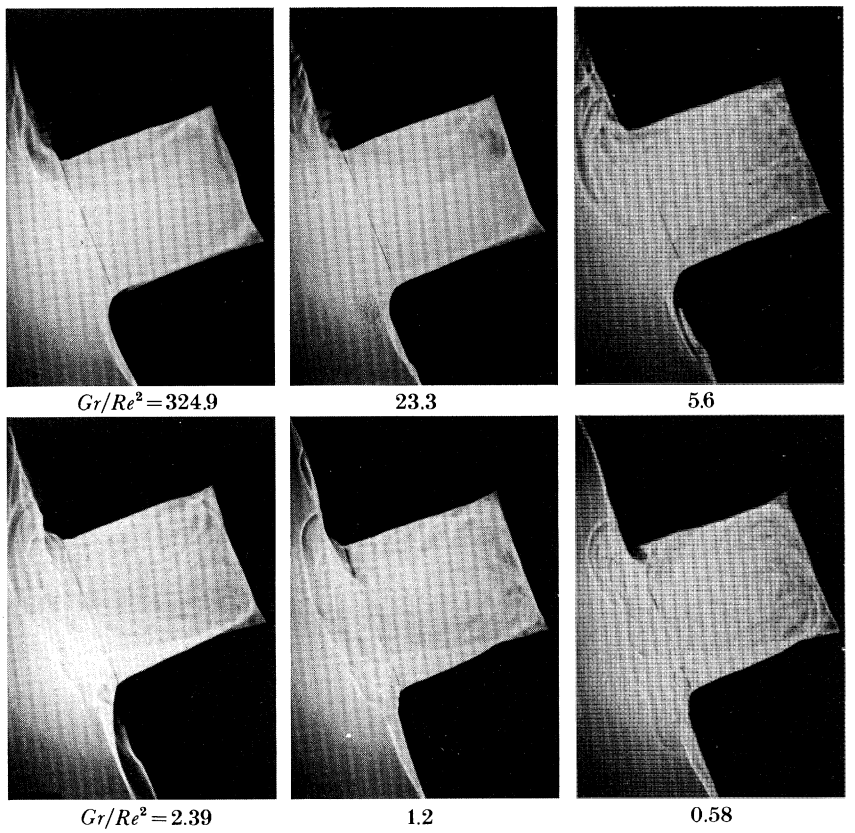

FIGURE 18. Shadowgraphs of heated-cavity flows with $a/b = 1.0$ and $\alpha = 20°$ for different values of Gr/Re^2: $Gr \approx 4.3 \times 10^7$, $\Delta T/T_\infty \approx 1.26$.

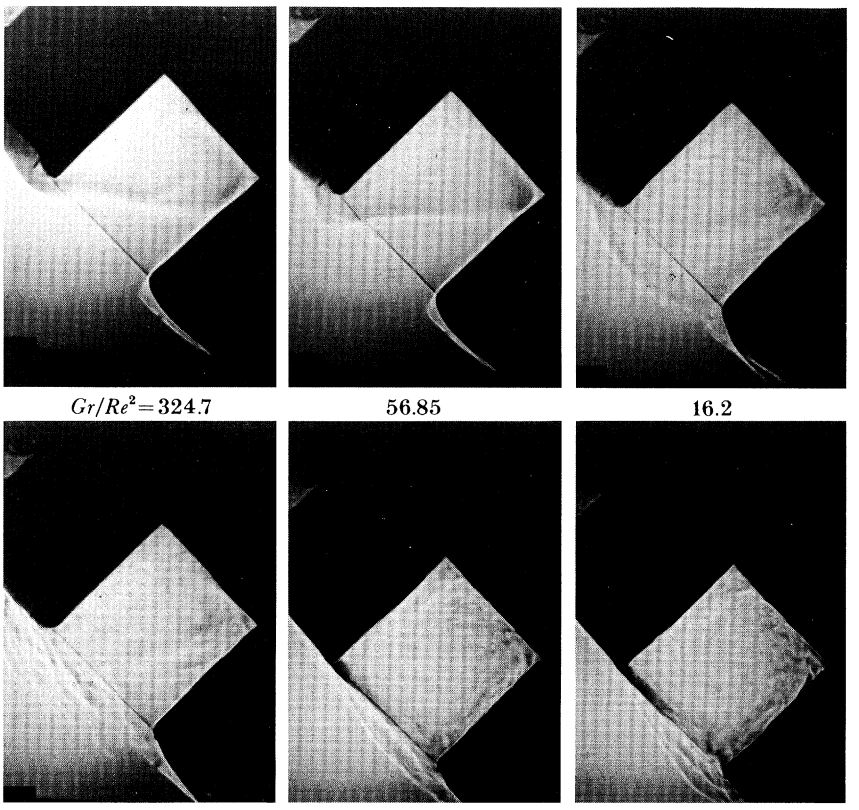

FIGURE 19. Shadowgraphs of heated-cavity flows with $a/b = 1.0$ and $\alpha = 45°$ for different values of Gr/Re^2: $Gr \approx 4.3 \times 10^7$, $\Delta T/T_\infty \approx 1.26$.

PHILOSOPHICAL TRANSACTIONS OF THE ROYAL SOCIETY A MATHEMATICAL, PHYSICAL & ENGINEERING SCIENCES

TABLE 1. TEST MATRIX OF EXPERIMENTAL CONDITIONS

			variable determined		
			U, V, W		
a/b	α		$\overline{u'^2}, \overline{v'^2}, \overline{w'^2}, \overline{u'v'}$	T	photographs
0.5	0°	$\Delta T/T_\infty$	1.2	1.18	1.18
		Gr	4.2×10^7	4.01×10^7	4.01×10^7
		Gr/Re^2	∞	459.8–0.56 and ∞	439.7–5.38 and ∞
	20°	$\Delta T/T_\infty$	—	1.18	1.18
		Gr		4×10^7	4×10^7
		Gr/Re^2		110.4–0.56 and ∞	683.6–0.55 and ∞
	45°	$\Delta T/T_\infty$	—	1.2	—
		Gr		4.06×10^7	
		Gr/Re^2		274–1.16 and ∞	
1.0	0°	$\Delta T/T_\infty$	1.19	1.19	1.19
		Gr	4.14×10^7	4.03×10^7	4.03×10^7
		Gr/Re^2	∞	225.3–0.55 and ∞	306.9–0.55 and ∞
	20°	$\Delta T/T_\infty$	—	1.26	1.26
		Gr		4.28×10^7	4.28×10^7
		Gr/Re^2		231.9–0.58 and ∞	324.7–0.58 and ∞
	45°	$\Delta T/T_\infty$	1.19	1.26	1.26
		Gr	4.2×10^7	4.27×10^7	4.27×10^7
		Gr/Re^2	∞	233.7–0.57 and ∞	324.7–0.58 and ∞
1.46	0°	$\Delta T/T_\infty$	—	1.24	1.24
		Gr		4.2×10^7	4.2×10^7
		Gr/Re^2		117.4–0.57 and ∞	718.9–0.57 and ∞
	20°	$\Delta T/T_\infty$	—	1.21	1.21
		Gr		4.09×10^7	4.09×10^7
		Gr/Re^2		701.6–0.58 and ∞	667.7–0.56 and ∞
	45°	$\Delta T/T_\infty$	—	1.2	1.2
		Gr		4.07×10^7	4.07×10^7
		Gr/Re^2		695.8–0.58 and ∞	662.2–0.56 and ∞

TABLE 2. INSTABILITY AND PLUME FORMATION ON BOTTOM WALL[a]

α	$-y/b = -(Gr_y/Gr_b)^{\frac{1}{3}}$			
	theoretical critical value (Chen & Tszoo 1982)	value inferred from exp (Rotem & Claassen 1969)	value inferred from exp (Pera & Gebhart 1973)	value for first visible plumes (this study)
0°	0.020	0.23–0.28	0.35	0.23–0.48
20°	0.037	—	probably > 1.0 (extrapolation)	0.39–0.54
45°	0.083	—	—	0.82

[a] Other authors present values of Gr_y. Value of Gr_b for this work is 4.2×10^7.

For $\alpha = 0°$, we can make a comparison with the experimental result of Rotem & Claassen (1969). Their result, $(Gr_y)^{\frac{1}{3}} = 80$–$100$, translates into $-y/b = 0.23$–0.28, in close agreement with our observed values. Similar agreement is found with the observations of Pera & Gebhart (1973). To adapt the results of authors who assumed $\Delta T/T_\infty \ll 1$ for theoretical purposes, or who did experiments with small overheat, we have based our Grashof number on ambient-temperature properties. Had we used properties evaluated at a mean film temperature, the corresponding values of $-y/b$ would be increased by about a factor of two.

PHILOSOPHICAL TRANSACTIONS OF THE ROYAL SOCIETY A MATHEMATICAL, PHYSICAL & ENGINEERING SCIENCES

We believe that this instability plays a key role in initiating the unsteadiness and eventually the turbulence seen in our cavity, even at relatively low Grashof numbers. At first, it was suspected that the inflexional instability of the separated flow near the bottom lip of the cavity might be the trigger for unsteadiness and a temporary turning vane was installed, to show what would happen when the separated zone was nearly eliminated. The flow became a little steadier as a result, but the thermally driven instabilities grew as before.

(iv) On the back wall there is a thin hot boundary layer into which the bottom boundary layer and some of the plumes emerging from the latter are entrained.

(v) A fairly sharp, stably stratified, roughly horizontal thermocline marks the bottom of a comparatively quiescent pool of hot air in the top of the cavity. This pool receives the back wall boundary layer and the plumes that have escaped entrainment. When $\alpha = 45°$, and to a lesser extent when $\alpha = 20°$, the discharge of the back wall boundary layer into this pool is very reminiscent of the bottom of a waterfall, but upside down.

(vi) A fairly sharply defined outflow from the hot pool separates from the upper edge of the aperture, reattaching soon thereafter, particularly when $\alpha > 0°$.

The flow visualization also gave a clear impression of the effects of a/b and α on the degree of unsteadiness of the flow. Our observations generally support the notion that the unsteadiness originates in the instability of the bottom boundary layer, as follows.

(*a*) Increase of α, at fixed a/b, generally reduced the degree of unsteadiness. As α increases, the onset of plume formation is moved toward the back wall, so that a smaller fraction of the cavity volume is involved with plume motion. Plumes formed near the rear of the cavity, at $\alpha = 20°$ and especially at $\alpha = 45°$, rise only a short distance before merging with the back wall boundary layer or penetrating the thermocline. This restricts the size and vigour of unsteady motions associated with the plumes.

(*b*) Increase of a/b, at fixed α, generally increases the degree of unsteadiness, especially at the lower values of α. It increases the fraction of cavity volume that can be involved with plumes, at least until the bottom of the back wall retreats beyond the line where the thermocline intersects the bottom wall. (This happens at $\alpha = 45°$, once a/b exceeds about 0.8.)

(*c*) Unsteadiness can be almost completely suppressed by increasing α and decreasing a/b. Thus for $\alpha = 45°$ and $a/b = 0.5$, the flow is almost perfectly steady.

In most cases, the hot air above the thermocline appeared to act as a sort of shock absorber, quickly reducing the vertical velocity of warm air parcels, which are positively buoyant below the thermocline and negatively buoyant above it. At $\alpha = 45°$ there was a prominent, nearly steady, penetrating and rebounding current where the back wall boundary layer enters this top layer. A stationary wave on the thermocline accompanies this structure, and is clearly seen in the lower right frame of figure 2. The current could be made more clearly visible with the smoke from $TiCl_4$ sticks.

3.1.2. *Measurements of temperature*

Typical mean temperature profiles across the aperture plane of a cavity with $a/b = 0.5$ are given in figures 3–5. In the figures, $\theta = (T - T_\infty)/(T_c - T_\infty)$. The profiles corresponding to $Gr/Re^2 = \infty$ (or $Re = 0$) are the ones of interest here. They display the following general characteristics.

(i) For all aspect ratios and inclination angles, steep temperature gradients and high levels of fluctuation are observed near the top and bottom of the aperture plane. The hot layer near

the bottom edge, which is associated with the separation of flow from that edge, is essentially independent of a/b, and becomes thinner as α is increased. The hot layer in the top third of the aperture plane is thickest when a/b and α are both largest. Its profile changes more with α, at fixed a/b, than vice versa. At $\alpha = 45°$, the entire temperature distribution is essentially independent of a/b.

(ii) The fluctuation levels, represented in the figures by bars of length twice the standard deviation, σ, are substantial in the region of high gradient, for all α and a/b. However, they decrease as α increases, especially in the lower layer. The fluctuations also diminish, particularly in the upper layer, when a/b is increased at constant α. This may be a result of the increasing volume of the 'shock-absorbing' hot pool, but with the data available it is risky to propose an explanation of these trends. We should be reminded, too, of the limited frequency resolution of these measurements.

(iii) Especially when $\alpha = 45°$, $\partial T/\partial x$ is very nearly constant across the upper heated flow, having a value of about 8850 K m^{-1}. If we assumed that the isotherms are nearly horizontal in this region, the vertical temperature gradient would be larger by a factor of $\sqrt{2}$. Taking the mean temperature to be about 475 K, we can estimate a Brunt–Vaisala frequency for the hot layer, of magnitude

$$N = (g/T\sqrt{2}\partial T/\partial x)^{\frac{1}{2}} \approx 16 \text{ Hz}.$$

This estimate is intended to give an upper limit to the frequency of internal waves that might propagate in this stably stratified region. It cannot be taken too seriously, because the region is also sheared, bounded by a nearly isothermal region on the bottom and by a steeply sloping roof above. Of special interest is the possibility of resonant standing-wave modes with horizontal wavelength equal to twice the length of the thermocline. A highly simplified linearized analysis in Humphrey *et al.* (1983) suggests that these would have frequencies in order $\frac{1}{3}N$ or $\frac{1}{4}N$. These preliminary ideas are relevant to a discussion of periodic, finite-amplitude oscillations observed in the mixed-convection régime.

3.1.3. *Measurements of velocity and turbulent stress components*

The bulk of the velocity and turbulent stress data were measured on the cavity symmetry plane $z = 0$ (figure 1). A limited number of measurements was also performed to check the degree of spanwise uniformity in the flow. These results strongly support the notion of a flow that is essentially two-dimensional in the mean. Earlier measurements of temperature by Humphrey *et al.* (1981) also revealed spanwise uniformity.

Flow through and in front of the aperture plane. Three configurations (see table 1) were selected for detailed exploration by laser–Doppler velocimetry. The results, obtained at the measurement locations shown in figure 6, are available in Humphrey *et al.* (1983) and only representative plots are provided and discussed here.

For clarification and comparison, figures 7–10 show the aperture-plane profiles of V and T, with 2σ bars superposed to indicate the fluctuation levels on the same scales; σ is the r.m.s. of the turbulent velocity fluctuations and not a measure of the random uncertainty in V, which is considerably smaller. The profiles emphasize the fact that these are highly fluctuating velocity fields and confirm the impression gained from flow visualization and temperature measurements that the fluctuations are most vigorous in the shallow cavity at $\alpha = 0°$ and least vigorous in the deep cavity at $\alpha = 45°$. Figure 10 directly compares the three $V(x)$ profiles, without the indications of fluctuation level.

PHILOSOPHICAL TRANSACTIONS OF THE ROYAL SOCIETY A MATHEMATICAL, PHYSICAL & ENGINEERING SCIENCES

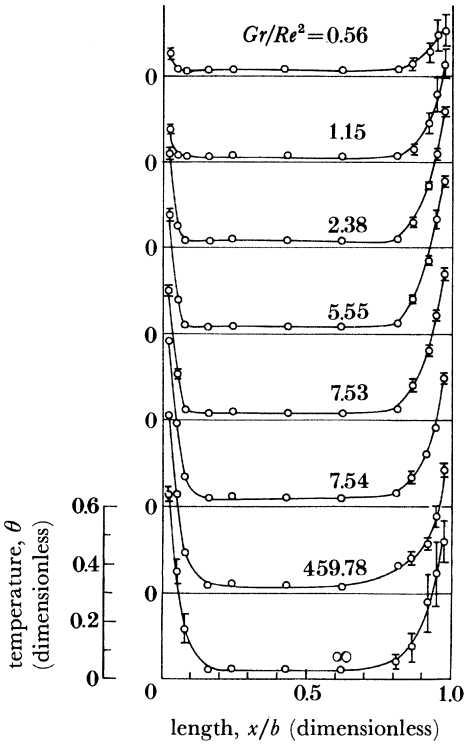

FIGURE 3. Cavity aperture-plane temperature distributions in mixed-convection régime for $a/b = 0.5$, $\alpha = 0°$, $\Delta T/T_\infty = 1.19$, $Gr = 4.02 \times 10^7$, $T_\infty = 298.2$ K.

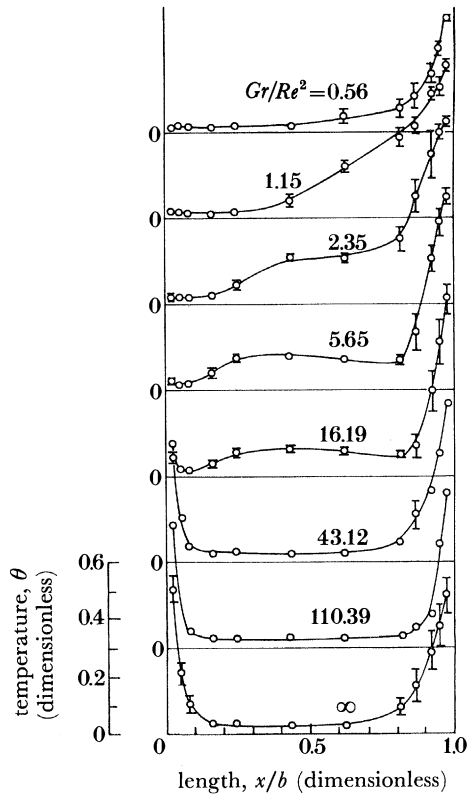

FIGURE 4. Cavity aperture-plane temperature distributions in mixed-convection régime for $a/b = 0.5$, $\alpha = 20°$, $\Delta T/T_\infty = 1.18$, $Gr = 4.0 \times 10^7$, $T_\infty = 295.8$ K.

PHILOSOPHICAL TRANSACTIONS OF THE ROYAL SOCIETY A MATHEMATICAL, PHYSICAL & ENGINEERING SCIENCES

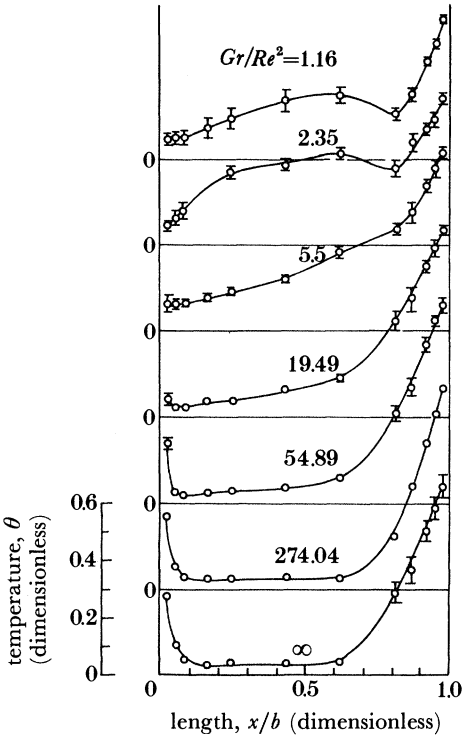

FIGURE 5. Cavity aperture-plane temperature distributions in mixed-convection régime for $a/b = 0.5$, $\alpha = 45°$, $\Delta T/T_\infty = 1.20$, $Gr = 4.06 \times 10^7$, $T_\infty = 294.1$ K.

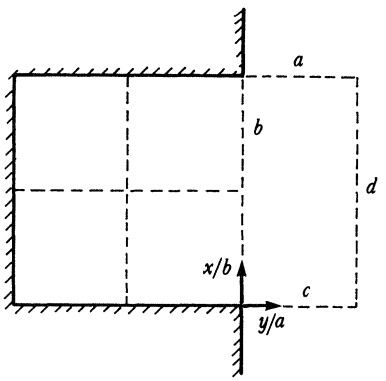

FIGURE 6. Position at which mean velocities and turbulent stress components were measured by using l.D.v. All positions, shown as broken lines in the figure, were located on the cavity symmetry plane $z/c = 0$.

An especially interesting feature is displayed by the profiles with $\alpha = 0°$. This is the extension of the bottom wall recirculating flow region past the aperture plane into the approaching outer flow. Note that the strength of inflow and outflow increase as a/b increases from 0.5 to 1.0, and then as α increases from 0° to 45°, but that the profiles become more nearly symmetric about $x/b = 0.5$ as this happens. Numerical integration shows that the net volume flow rate out of the cavity displays just the opposite trend. Time-averaged streamline fields of the flow in the region just in front of the cavity are given in Humphrey *et al.* (1983).

Several features of the measured turbulent stress component (not shown here because of space limitations) deserve comment.

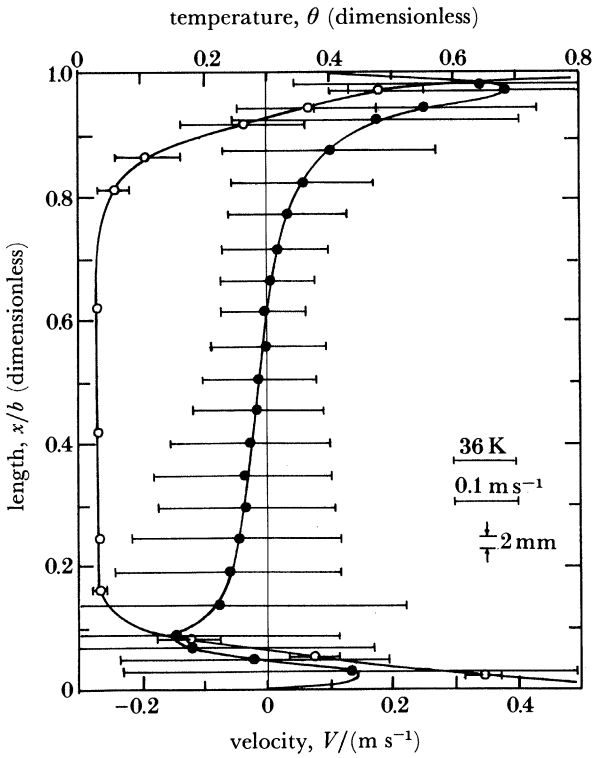

FIGURE 7. Measurements of θ (○) and the V velocity component (●) in the cavity aperture plane with 2σ levels shown. Data correspond to $a/b = 0.5$, $\alpha = 0°$.

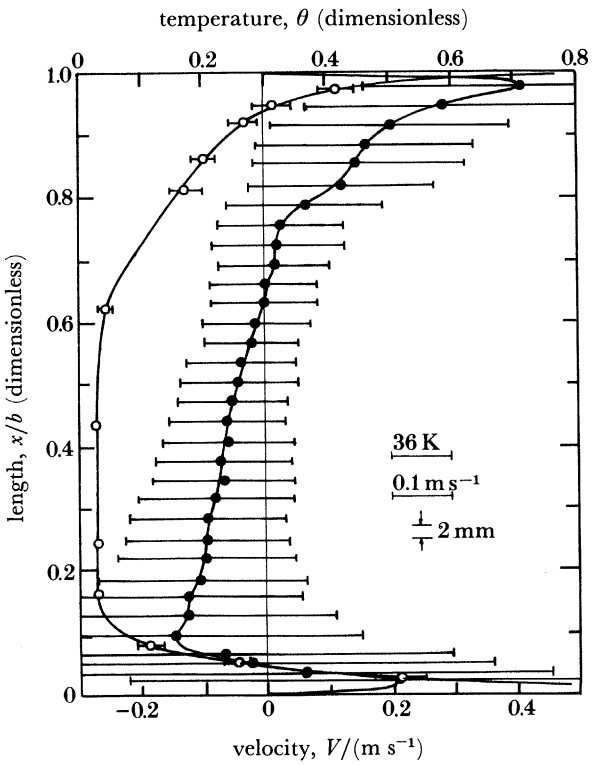

FIGURE 8. Measurements of θ (○) and the V velocity component (●) in the cavity aperture plane with 2σ levels shown. Data correspond to $a/b = 1.0$, $\alpha = 0°$.

PHILOSOPHICAL TRANSACTIONS OF THE ROYAL SOCIETY A MATHEMATICAL, PHYSICAL & ENGINEERING SCIENCES

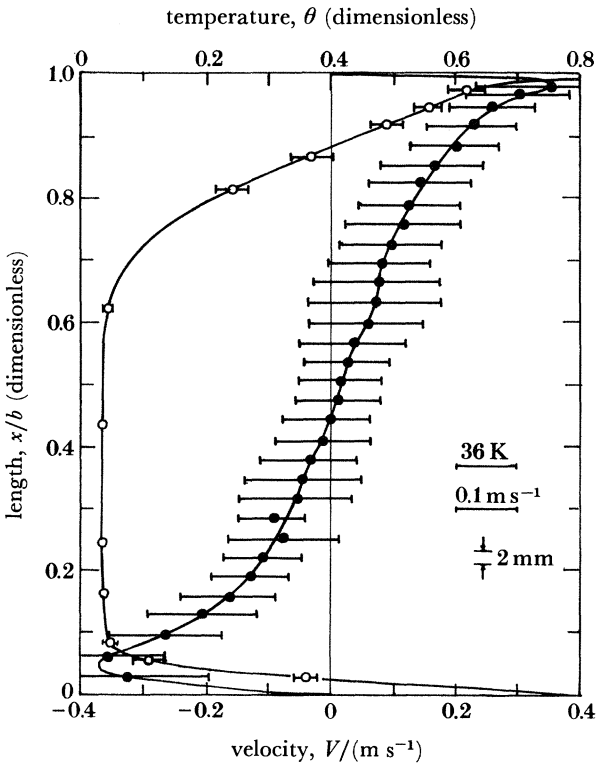

FIGURE 9. Measurements of θ (○) and the V velocity component (●) in the cavity aperture plane with 2σ levels shown. Data correspond to $a/b = 1$, $\alpha = 45°$.

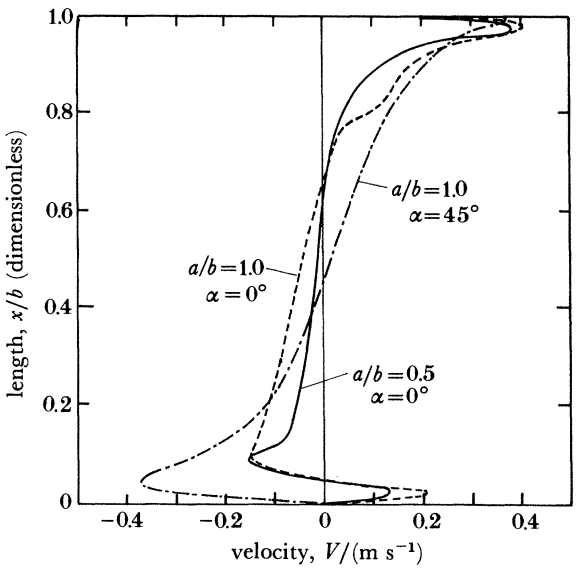

FIGURE 10. Composite of the V velocity profiles given in figures 7–9.

(i) The flow, entering from below, across the outward extension of the bottom wall ($x/b = 0$, $y > 0$) was virtually devoid of the turbulent shear stress $-\rho\overline{u'v'}$, although it was highly sheared out to about $y/a = \frac{1}{8}$. By contrast, $\rho\overline{u'v'}$ reached substantial values on the corresponding extension of the top wall.

(ii) The turbulent kinetic energy was by no means isotropically distributed anywhere in the

flow. There were striking increases in the horizontal components $\overline{v'^2}$ and $\overline{w'^2}$, but usually a slight decrease in the vertical component $\overline{u'^2}$ in the stably stratified region $x/b > \frac{2}{3}$. Even at $\alpha = 45°$, where u' and v' were equally inclined to the vertical, $\overline{u'^2}$ was systematically quite a bit smaller than either $\overline{v'^2}$ or $\overline{w'^2}$. Of course, these observations must be accepted with caution, because of the 'false turbulence' which can appear in l.D.v. data when there are large fluctuations in the index of refraction. The characteristically lower values of $\overline{u'^2}$ were observed, however, even well in front of the cavity, where the laser beams were traversing mostly isothermal air.

(iii) To the extent that we can estimate $E_{xy} = \partial V/\partial x + \partial U/\partial y$ along the aperture plane and along the outward extensions of the top and bottom walls, we infer the following relation between $\overline{u'v'}$ and E_{xy}. (*a*) Along $x/b = 0, y/a > 0.02$: $E_{xy} < 0$, while $\overline{u'v'} \approx 0$; (*b*) along $x/b = 1$, $y/a > 0.04$: $E_{xy} < 0$ while $\overline{u'v'} > 0$; (*c*) in the upper half of the aperture plane: $E_{xy} > 0$ while $\overline{u'v'} > 0$; (*d*) in the lower half of the aperture plane, where $0.05 < x/b < 0.5$, $E_{xy} > 0$ while $\overline{u'v'} < 0$; (*e*) very close to the bottom wall, but on the upper side of the separation bubble, $E_{xy} < 0$ while $\overline{u'v'} > 0$.

Qualitatively, these relations imply a positive eddy viscosity, $-\rho\overline{u'v'}/E_{xy}$, in the regions of unstable or ineffectual density stratification, but a negative eddy viscosity in regions of strong stable stratification. In the latter regions the product $-\overline{u'v'}E_{xy}$, which ordinarily is positive and represents a transfer of kinetic energy from the mean-flow account to the eddy account, is locally negative and thus represents a reverse transfer. Such a transfer has been shown to take place in stably stratified shear layers, in the vicinity of the critical layer, at which the flow speed and the speed of internal waves coincide. The linearized model of internal waves, given in Humphrey *et al.* (1983), yields wave speeds in the range 0.1–0.3 m s^{-1}. Because these lie in the range of our measured values of V, it is possible that we are seeing something like the absorption of internal waves at a critical layer; see Booker & Bretherton (1967).

Inner flow. Limited, single-component measurements of the flow inside a cavity with aspect ratio $a/b = 1$ were obtained for conditions of $\alpha = 0°$ and $\alpha = 45°$ respectively. As shown in figures 11–14, the measurements were taken along the planes $x/b = 0.5$ (U component) and $y/a = -0.5$ (V component). For the case $\alpha = 0°$, only unweighted data are available. Interception of the laser beams by the top wall in the cavity impeded the near-wall measurements in this region of the flow. Likewise, beam deflection due to refractive index gradients precluded making measurements very near the back and bottom walls. The results are in accordance with the observations made earlier. For both inclination angles the V-component profiles in figures 11 and 13 display the flow reversals corresponding to the separated recirculating flow region on the bottom wall. The profiles show clearly that increasing α decreases the size of the recirculation zone and strongly damps turbulent fluctuations inside the cavity.

3.1.4. *Convective heat transfer*

Humphrey *et al.* (1983) document and criticize an attempt to extract estimates of convective heat-transfer rates from the V profiles in the aperture plane. Because the method places extreme demands on the accuracy of V, and on the two-dimensionality of the flow, the results, although qualitatively correct, are inconclusive and an adequate discussion is beyond the proper scope of this paper.

PHILOSOPHICAL TRANSACTIONS OF THE ROYAL SOCIETY A MATHEMATICAL, PHYSICAL & ENGINEERING SCIENCES

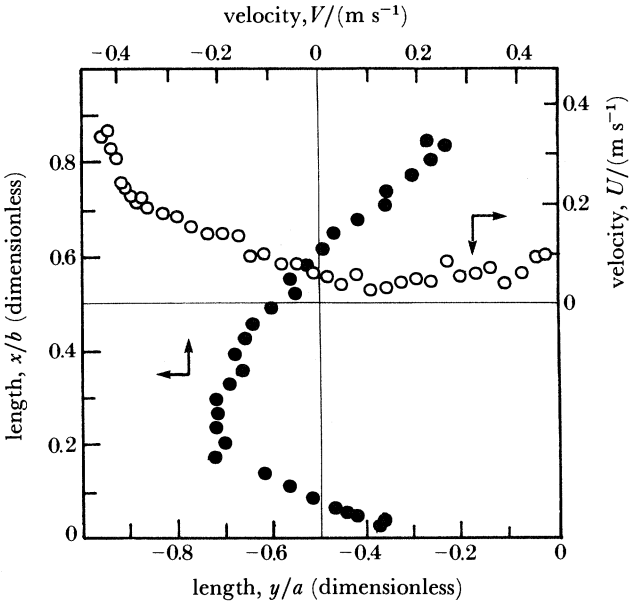

FIGURE 11. Mean velocity measurements inside the cavity on the symmetry plane, $z/c = 0$, with $a/b = 1.0$ and $\alpha = 0°$; unweighted data. Measurements on planes shown.

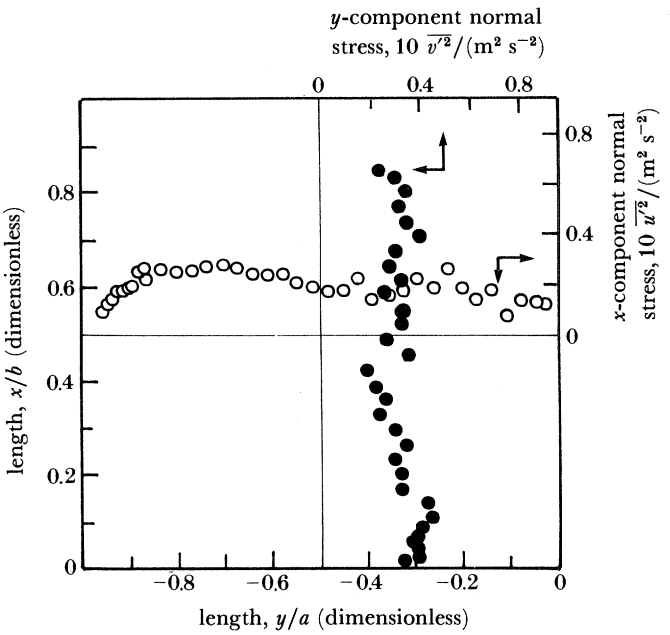

FIGURE 12. Normal stress measurements inside the cavity on the symmetry plane, $z/c = 0$, with $a/b = 1.0$ and $\alpha = 0°$; unweighted data. Measurements on planes shown.

3.2. *Mixed convection*

Before discussing the experimental results for mixed convection, we consider a very rough model of the purely forced flow. Figure 15 shows the distribution of velocity over the upstream face of an inclined flat plate, in two-dimensional potential flow. The flow surrounds both the plate and a dead-air wake, in which the pressure is that of the unperturbed stream. The location of the stagnation point, relative to the shaded section of the plate (which represents the position

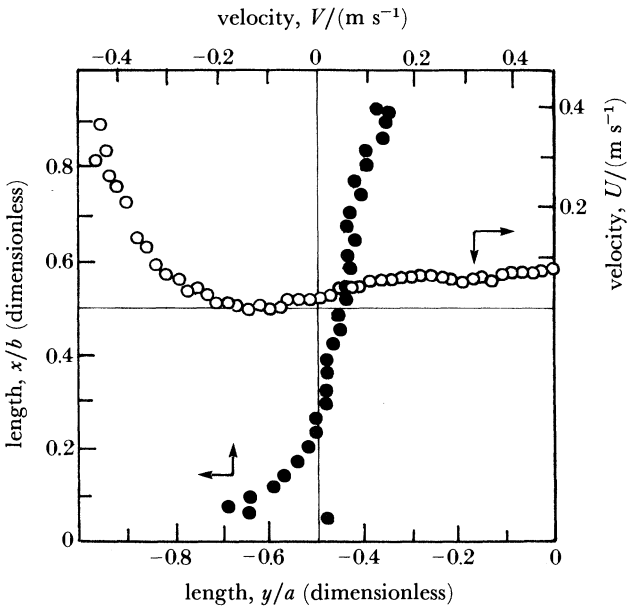

FIGURE 13. Mean velocity measurements inside the cavity on the symmetry plane, $z/c = 0$, with $a/b = 1.0$ and $\alpha = 45°$. Measurements on planes shown.

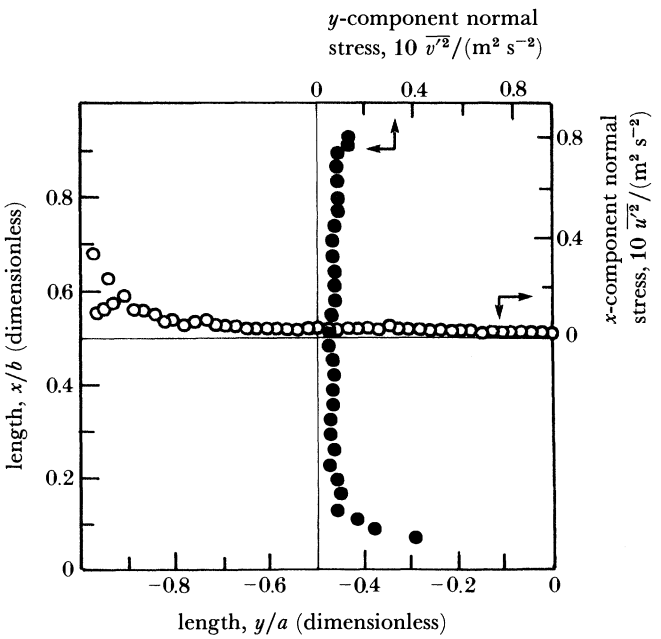

FIGURE 14. Normal stress measurements inside the cavity on the symmetry plane, $z/c = 0$, with $a/b = 1.0$ and $\alpha = 45°$. Measurements on planes shown.

of our cavity opening) is the principal feature of interest. A comparable theoretical calculation for a plate indented by an upstream-facing cavity would be quite difficult, but it seems intuitively clear that the presence of the cavity would displace the stagnation point slightly away from the cavity.

The influence of the finite length of the cavity along its axis of rotation is potentially quite

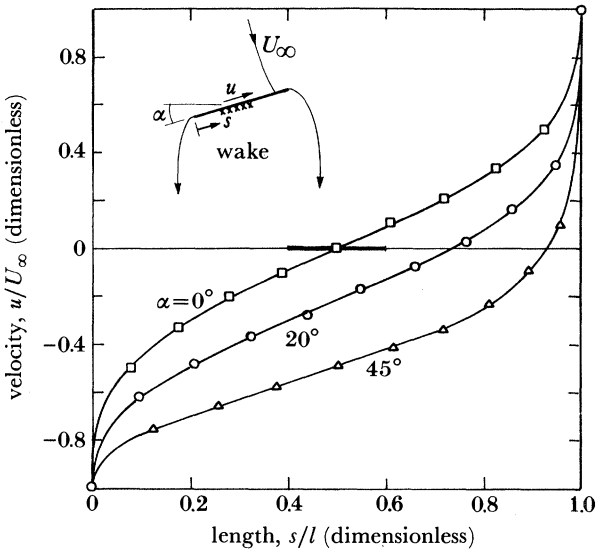

FIGURE 15. Potential flow along a flat plate of length l inclined at an angle $90°-\alpha$ with respect to the approaching wind, U_∞.

important. While b/c is small, the aspect ratio of the cavity plus its upward and downward extensions (see figure 1) is not small and the forced flow is bound to be significantly three-dimensional. Near the aperture plane, the resulting z component of velocity will be, very approximately, $W \approx U(z/c)\cos\alpha$ for $z/c < 0.35$, increasing more steeply thereafter, to $W \approx \pm U\cos\alpha$ at $z = \pm\frac{1}{2}c$. This lateral flow divergence would presumably increase V somewhat in the region just in front of the cavity. More importantly, in the mixed flow, this divergence will stretch the vortex lines associated with the buoyancy-driven convection.

3.2.1. *The experimental results*

There were three general results of phenomenological interest:

(i) a general stabilizing effect of weak winds;

(ii) periodic, two-dimensional oscillation of the cavity flow, in the presence of weak winds;

(iii) migration of the stagnation points of the time-averaged flow, resulting from the competition between free and forced convection when $\alpha = 20°$ and $45°$.

3.2.2. *Qualitative effects of very weak winds*

The most surprising and thought-provoking result of the mixed convection experiments occurred with very weak winds, $U_\infty \approx 4$–6 cm s^{-1}. These winds strongly inhibited the chaotic and three-dimensional fluctuations that characterized most of the free convection flows, leading to flows that were either almost perfectly steady, or periodically oscillating. The effect was first noticed when the forced flow was dying away after power to the blower was cut off. One could monitor the deceleration by noting the orientation of a small plume of hot air that was originally swept downstream by the forced flow. When the plume was inclined about 10°–30° downstream, the flow in the cavity would be dramatically stabilized. Just after the plume became vertical, the cavity flow would burst into irregular fluctuations, which persisted until the blower was started again.

The wind tunnel speed was then held steady in the range 4–6 cm s^{-1} and quantitative evidence of the reduction of fluctuations was obtained. This appears in the contrast between the bottom two temperature profiles in each of figures 3–5. The bottom profiles is for free convection; the next profile shows the effect of the weak wind. The cavity flow was not made perfectly steady, but fluctuations became either very periodic, or very few and far between. Because the temperatures were sampled periodically, at a frequency nearly equal to an integral fraction of the oscillation frequency, a striking reduction of the variance of the temperature samples does not necessarily discriminate between the steady flows and the periodic ones.

It seems likely that weak horizontal winds stabilize the cavity flow by two separate but cooperating mechanisms.

(i) They carry away those wisps of vorticity that would otherwise separate from the bottom edge of the aperture-plane extension and be carried into the cavity by the buoyancy-induced flow. These might not be vigorous enough to be noticed by themselves, but might serve to trigger instabilities in the boundary layer on the heated bottom wall.

(ii) By stretching the vortex lines of the two-dimensional buoyancy-induced flow, they may inhibit the onset of the three-dimensional instabilities, to which the bottom boundary layer is first subject (Chen & Tszoo 1982). At the same time, they could enhance local concentration of spanwise (z component) vorticity, which is essential to the onset of the oscillating two-dimensional instability, allowing it to reach finite amplitude first, even on nearly horizontal surfaces (Pera & Gebhart 1973).

It is impossible to put these suggestions on a firm base of experimental facts, with the few and mostly qualitative observations we have, or to see theoretically just how the vortex stretching would work inside the cavity, where it must be inhibited by the glass windows. We simply record them here, hoping to stimulate interest in the problem.

3.2.3. *Periodic oscillations*

The periodic oscillations shown in figure 16, plate 2 seem to be the natural outcome when α was between 0° and 20° and a/b was 0.5 or 1.0. The oscillation frequencies were measured either by displaying a prominently fluctuating wire temperature on a chart recorder, or by 'freezing' the shadowgraph image with stroboscopic illumination. The frequencies fell in the range 2.2–5 Hz, and the oscillating flows seemed quite two-dimensional. (With only shadowgraph images, we could not definitely distinguish between two-dimensional flows and flows that might have a periodic waviness in z.) The amplitude of oscillatory motion was highest near the top of the aperture plane, where well formed blobs of hot air were periodically expelled from the cavity. A synchronous flapping of the back wall boundary layer and of the rearward part of the bottom boundary layer was usually noticeable. Temperature fluctuations in the heated portion of the inflow, near the bottom of the aperture plane, were dramatically reduced.

Unfortunately, time and research priorities did not permit a comprehensive delineation of the parameter space in which oscillatory behaviour occurs. However, a tabulation of such data as we gathered with an attempt to interpret the results is given in Humphrey *et al.* (1983). Although the reason for such prominent oscillatory behaviour is not conclusively demonstrated, some possibilities have been identified and others have been tentatively eliminated. The scenario that we believe to be most likely involves a resonant sloshing motion of the upper, stably stratified layer, in response to periodic impulses delivered to that layer at the rear of

the cavity. These impulses would arrive as a consequence of an oscillatory instability of the bottom boundary layer, being transmitted mainly via a modulated momentum flux in the back wall boundary layer. Because the distance between these layers was not large compared with the observed wavelength of the sloshing motion, an effective feedback loop via the pressure field may be a component of the observed process. We find that either one of two distinct mechanisms, (i) barotropic instability of the separated shear layer at the lower lip of the cavity and (ii) baroclinic instability of the bottom boundary layer, could conceivably trigger the observed oscillations, but we cannot conclude that one alone is responsible. Further experimentation, to delineate the exact range of parameters in which the oscillations appear and to determine whether they are two-dimensional or three-dimensional, would probably settle the issue.

3.2.4. *Movement of the stagnation lines; escape of the heated air*

Figures 17–19 (plates 3 and 4) are representative shadowgraphs for the mixed convection régime. A broad and relevant question about the mixed convection flows is to consider by what path heated air escapes from the cavity. If we believe the flow to be essentially two-dimensional, we are led to pay special attention to the occurrence and migration of stagnation lines of the time-averaged velocity field, and to the stream surfaces that arrive at or depart from these stagnation lines.

In this section, we pursue this point of view until some of its inevitable conclusions are seen to conflict seriously with our measured temperature profiles and with the implications of some of the shadowgraph pictures. We then retrace parts of the argument, with the assumption that convection along the z axis plays an essential role.

Figure 20 displays sketches, intended to show the time-average streamlines and the regions occupied by heated air, in the three qualitatively distinct régimes of mixed flow that arise when $\alpha > 0°$. The sketches were guided by the assumption that the shadowgraph images result from gas conditions that are at least statistically independent of z. For example, we infer from figure 19, that there is heated fluid at any x in the aperture plane, for $Gr/Re^2 < 16.2$, because we see evidence of light refraction on both sides of the aperture plane. The sketches make no attempt to indicate the effects of cavity depth, which seems to have little influence on the migration of the stagnation lines.

The two-dimensional interpretation. Figure 20*a* shows the cavity at $\alpha = 20°$, in pure free convection. The flow entering the cavity is drawn up mostly from below, to replace the hot air that is propelled upward by a hydrostatic pressure gradient which exceeds the local specific weight. This flow is quite two-dimensional.

Figure 20*b* shows the first effects of a very weak wind. Two new stagnation points appear, one (O) where the oncoming wind divides, to go upward or downward, outside of the rising buoyant flow. The other (O′) appears on the wall below the cavity, at a point below which the flow is nowhere buoyant. The upward drift along the lower wall is entirely overwhelmed by the local forced flow, which accelerates as the bottom edge of the aperture-plane extension is approached. The process by which this happens when the forced flow is started may be imagined as a sequence of events as follows:

(i) A velocity field approximately identical to a potential flow over the unheated apparatus is suddenly superposed on the weak updraft of the free convection flow.

(ii) This produces an illegal downward slip velocity at the wall, which is countered by the introduction there of a compensating vortex sheet.

PHILOSOPHICAL TRANSACTIONS OF THE ROYAL SOCIETY A MATHEMATICAL, PHYSICAL & ENGINEERING SCIENCES

(iii) This new vorticity diffuses out to form the new boundary layer, cancelling the pre-existing vorticity of opposite sign, which was in the boundary layer of the induced flow.

Because the upward velocity of the induced flow decreases while the downward velocity of the forced flow increases, as distance down from the cavity increases, the weakest steady wind obtainable with the wind tunnel suffices to make O′ appear somewhat on the wall, as shown. The supply of fluid to the cavity then comes through a narrow stream channel, just below the stagnation streamline that leads to point O.

The effects of the forced flow between O and the upper lip of the cavity are too weak (the forced flow is locally much slower, and the pressure gradient weaker, than at O′) to block the upward escape of the hot air. This flow can be quite steady, or oscillating but still quite laminar.

The situation depicted in figure 20*b* persists as Re^2/Gr is increased until, quite suddenly, the mean situation changes to that shown in figure 20*c*. Stagnation point O has moved to the wall, the upward escape of hot air is cut off by the new stagnation (or separation) line O″, and a trapped vortex appears in the cavity. Hot air still escapes from the cavity, but it must now be transferred across the mean flow streamlines by vigorous turbulent eddying and it now escapes downward.

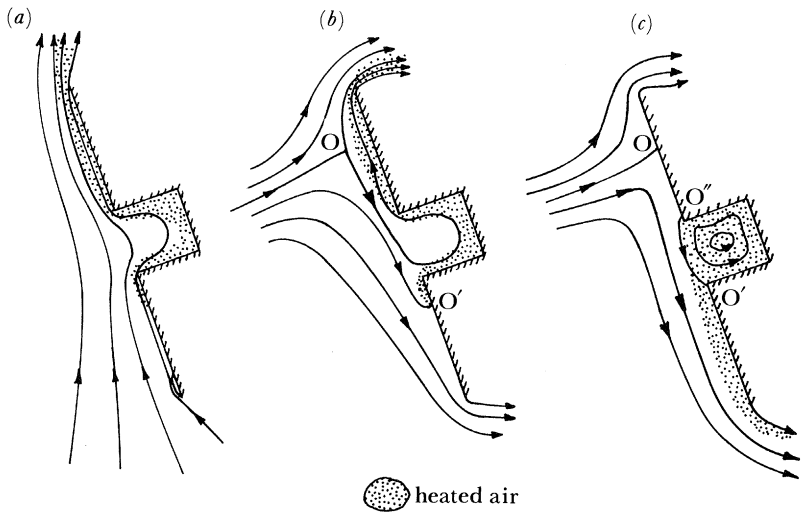

FIGURE 20. Qualitative options for two-dimensional free-forced flow. (*a*) No wind: $Gr/Re^2 = \infty$; (*b*) Weak wind: $10 < Gr/Re^2 < 500$; (*c*) Strong wind: $Gr/Re^2 < 10$.

To imagine how O″ would appear in a transient process, in which an adequately strong wind is suddenly started, we can add one more effect to the scenario described above for the lower wall. This is a reduction of the x direction 'buoyancy force' from $(\rho_\infty - \rho)\, g \cos\alpha$ to $(\rho_\infty - \rho)\, g \cos\alpha + \rho_\infty U\, \mathrm{d}U/\mathrm{d}x$, where U is the forced flow velocity just outside of the thermal boundary layer. Between O and the upper lip of the cavity, $U\, \mathrm{d}U/\mathrm{d}x < 0$.

It is hard to predict the point at which the upward motion of the hot air will be reversed, but it is relatively easy to see why the new stagnation point, O″, suddenly appears near the upper lip of the cavity, instead of moving slowly down from the vicinity of O as the wind speed is increased. Both U, which determines the amount of vorticity introduced at the wall, and $U\, \mathrm{d}U/\mathrm{d}x$, which reduces and eventually reverses the baroclinic generation of vorticity in the heated air, increase in absolute value from O to the lip. Thus the local obstacles to upward

progress of the hot air are, for a given wind speed, highest at the lip. If the hot air has sufficient inertia and residual buoyancy to pass the point where O″ is sketched, it may then continue up to O, past which point the forced flow helps it along. This is not to deny that a gradual movement of O″ might appear in a set of careful experiments designed to reveal it, but to explain why we saw so little movement either as a function of U_∞, or as the result of temporary additions to the aperture plane extensions.

A rough upper estimate of the value of U_∞ above which O″ appears can be made by setting $(\rho_\infty - \rho)\, g \cos\alpha + \rho_\infty U \mathrm{d}U/\mathrm{d}x = 0$ and relating $U\,\mathrm{d}U/\mathrm{d}x$ to U_∞^2/b and x/b by use of the potential flow calculations that produced figure 15. This gives $U_\infty \approx 4.4$ m s^{-1} for $\alpha = 20°$ and $U_\infty \approx 2.4$ m s^{-1} for $\alpha = 45°$, if we set $\rho = 0.5\,\rho_\infty$. These values are about eight times the corresponding observed values.

Discrepancies in the two-dimensional interpretation. A clear implication of the above interpretation of the shadowgraphs is that we should find elevated mean temperatures and large temperature fluctuations in the lower part of the aperture plane, under conditions corresponding to figures 20*b* and *c*. This expectation is not borne out by our temperature data, as is shown dramatically for $\alpha = 20°$ in the upper curve of figure 4 for $a/b = 0.5$ and corresponding measurements for $a/b = 1$ and 1.46. The data show that at $z = 0$, $T \approx T_\infty$ over much of the aperture plane, and that the extent of the ambient temperature region increases rather rapidly with increasing U_∞, (and somewhat with increasing a/b) once $Gr/Re^2 < 6$.

A second embarrassment is implied by details shown particularly vividly in, for example, figure 18. Note that the curves of light and dark, which we identify roughly with material surfaces, appear to spiral inward toward a vortex centre. If these snapshots indicate a quasi-steady state of affairs, material surfaces would coincide approximately with stream surfaces, and fluid, both hot and cold, would appear to be moving in toward the vortex centre. This would violate the continuity equation in a strictly two-dimensional flow, but not in one featuring a finite value of $\partial W/\partial z$.

A three-dimensional interpretation. Figure 21 presents a fairly speculative idea of what may actually be happening in the flows shown in the bottom row of shadowgraphs, in figure 18. Ambient air enters the cavity at points such as A and A′ and passes under and behind the main vortex. If it enters close to the bottom wall it is heated by conduction. Throughout most of the span of the cavity, the pressure is low in the vortex core and a particle path spirals slowly inward while drifting toward the nearer side window. The spanwise flow in the vortex core is arrested by the window and something akin to a vortex breakdown or explosion may occur close to the windows. (The theoretical possibilities of such a situation have been analyzed by Serrin (1972). What we suggest here is akin to Serrin's 'second kind of motion'.) This weakens or even reverses the radial pressure gradient, so that the particle suddenly spirals out again. The outer edges of the exploded vortex are responsible for the light refraction seen in those regions where the centrally located thermocouples register only ambient temperatures.

In a shallow cavity and at lower wind speeds, the central body of the vortex may extend out to the aperture plane, leaving a corresponding signature on the mean temperature distribution. This is seen prominently in figures 4 and 5, in which a local minimum in $T(x)$ appears around $x/b = 0.8$ (at $Gr/Re^2 = 2.35$ and 1.18 when $\alpha = 45°$ and at $Gr/Re^2 = 16.19$ and 5.65 when $\alpha = 20°$). One can speculate that this marks the average location of the main tongue of ambient temperature fluid, which wraps completely around the vortex core before being warmed by conduction.

PHILOSOPHICAL TRANSACTIONS OF THE ROYAL SOCIETY A MATHEMATICAL, PHYSICAL & ENGINEERING SCIENCES

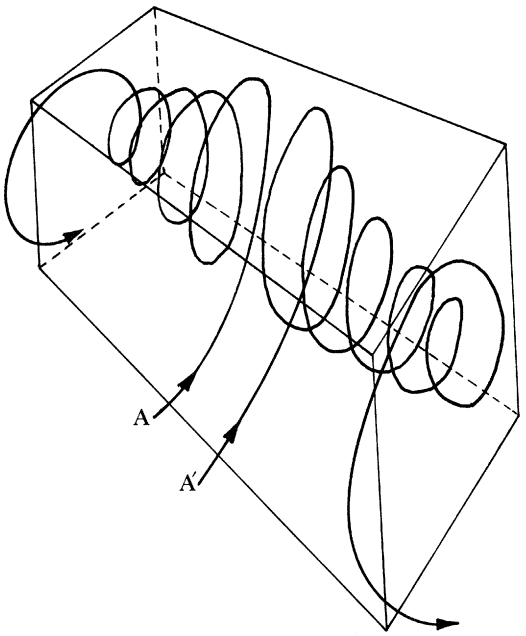

Figure 21. A three-dimensional interpretation of flow in the cavity for $Gr/Re^2 < 10$.

At higher wind speeds and in deeper cavities, the main vortex is pushed back away from the aperture plane and leaves no identifying thermal signature there.

One implication of the above interpretation, should it prove correct, is that results obtained by simulating the mean flow with a computational scheme that accommodates only two-dimensional motion are bound to differ from the real three-dimensional flow.

4. Comments on experimental accuracy

Humphrey *et al.* (1983) present a lengthy analysis of uncertainties in the temperature and velocity data. Some of their conclusions for the latter are of sufficiently general interest to merit mention here.

(i) Transmission of the laser beams through an extended region of fluctuating, non-uniformly heated air produced substantial levels of 'false turbulence' in our data. In future work of this sort, serious consideration should be given to the possible use of fibre optics, or the implementation of a comparator technique, in which the beams can be alternately directed at the target point in the air and at a nearby stationary target, perhaps a tautly strung wire.

(ii) The statistical effects of non-uniform seeding are potentially quite serious in this work, because of the very large fluctuation levels of both velocity and air density. It does not seem possible to predict these effects without independent data on the spatial distribution of particles, although it might be helpful to record the time intervals between individual velocity measurements. Simultaneous optical measurements of air velocity and air density (perhaps by Rayleigh scattering) are highly recommended.

5. Conclusions

(i) In pure free convection the time-averaged flow is, as hoped, very nearly two-dimensional. Specifically, no systematic variation of W or U as a function of z was found in the aperture plane, for $-\frac{1}{6}c \leqslant z \leqslant +\frac{1}{6}c$ and in this same region no statistically significant non-zero value of W was found. The instantaneous flow is unsteady and three-dimensional, the velocity fluctuations being large compared with the mean velocities in many parts of the flow.

(ii) Downward inclination of the cavity reduced the relative level of fluctuations, primarily by reducing both the severity of flow separation from the lower lip of the cavity and the baroclinic instability of the boundary layer on the bottom wall. Many of the observed trends seemed consistent with those found by Rotem & Claassen (1969) and by Pera & Gebhart (1973) in studies of flow above a horizontal or slightly inclined flat plate.

(iii) Mean velocity and temperature profiles are determined with sufficient accuracy to establish significant targets for a demonstration of the effectiveness of computational simulations, but with too little accuracy to permit reliable estimation of the net convective heat transfer. The dominant sources of uncertainty are associated with the possibilities of non-uniform seeding, fluctuations in index of refraction and very weak flows in the spanwise direction.

(iv) When the cavity is faced into a very gentle wind ($U_\infty \approx 4$–6 cm s^{-1}), the irregular unsteadiness of the flow is greatly reduced. The result may be either a very nearly steady flow, or a flow that oscillates very periodically, with a frequency ranging from 2–5 Hz. The oscillations may be mostly two-dimensional, but our observations do not rule out a spanwise modulation of phase, which might be expected in the light of the work of Pera & Gebhart (1973) and the stability theory of Chen & Tszoo (1982).

When $\alpha = 20°$ and $45°$, these weak winds cut off the induced flow from below, which is the main supply of ambient air entering the cavity in pure free convection. The new supply comes from a layer just below the dividing stream-surface of the forced flow. The hot air escapes upward from the cavity, as in free convection.

(v) Stronger winds cause major discrepancies between our temperature data and any interpretation of the shadowgraph pictures that assumes two-dimensional flow. The upward escape of hot air is blocked by the locally downward-forced flow and any direct escape downward seems kinematically unlikely and has escaped experimental detection. It seems likely that ambient air rushes directly into the lower part of the aperture plane, rises behind a major coherent vortex, is wrapped around and entrained into the vortex, together with heated, vorticity-bearing fluid from the outer regions of the boundary layers. The air drifts towards the nearer side window while spiralling around the vortex until, near the window, the vortex 'explodes' in a manner akin to the 'second kind of flows' discussed by Serrin (1972). The air then escapes from the cavity near the side windows, being cast out like sparks from a pinwheel.

5.1. *Recommendations*

The work has revealed many problems that deserve more detailed investigation. Several of these have to do with the use of l.D.v. in strong free convection flows. The use of fibre optics to minimize displacement and false turbulence effects resulting from beam dancing looks promising. Should it fail, work could be done on a comparator technique, in which a fine wire stretched tautly along the nominal path of a velocity survey could serve as a local stationary scattering target.

PHILOSOPHICAL TRANSACTIONS OF THE ROYAL SOCIETY A MATHEMATICAL, PHYSICAL & ENGINEERING SCIENCES

Panoramic observations of the scattering-particle density field, by use of a thin sheet of laser light, would help to set at rest or to emphasize, worries about non-uniform seeding. Simultaneous density and velocity measurements, by using Rayleigh scattering as a measure of air density, are being attempted in a number of laboratories. When developed, these would seem to offer essential advantages for l.D.v. work in flows such as ours.

It would certainly be interesting to perform a more comprehensive mapping of the conditions that lead to periodic oscillations and conduct flow-visualization studies that reveal spanwise variations. It would be easy, and potentially very interesting, to investigate the effect of spanwise solid extensions of the aperture plane, to make the forced flow more nearly two-dimensional.

This investigation was supported by Sandia National Laboratories, Livermore, California, through contract no. 20-1012. We are pleased to acknowledge the constant interest and encouragement received from our colleagues at Sandia. The authors' names appear in alphabetical order.

References

Booker, J. R. & Bretherton, F. P. 1967 The critical layer for internal gravity waves in a shear flow. *J. Fluid Mech.* **27**, 513–519.

Buchhave, P., George, W. K., Jr & Lumley, J. L. 1979 The measurement of turbulence with the laser–Doppler anemometer. *A. Rev. Fluid Mech.* **11**, 443–503.

Chen, K. S. 1983 Experimental investigation of strongly heated open cavity flow. Ph.D. thesis, University of California, Berkeley.

Chen, K. S., Humphrey, J. A. C. & Miller, L. 1983 Note on the pulsating nature of thermally driven open cavity flow. *Int. J. Heat Mass Transfer* **26**, 1090–1093.

Chen, T. S. & Tzsoo, K. L. 1982 Vortex instability of free convection flow over horizontal and inclined surfaces. *J. Heat Transfer* **104**, 637.

Drain, L. E. 1980 *The laser doppler technique*. New York: Wiley.

Eyler, L. L. 1980 Predictions of convective losses from a solar cavity receiver. *Paper no. 80-C2/SQ1-8, presented at the Century 2 Solar Energy Conference, San Francisco, California.*

Hess, C. F. & Henze, R. H. 1984 Experimental investigation of natural convection losses from open cavities. *J. Heat Transfer* **106**, 333–338.

Humphrey, J. A. C., Sherman, F. S. & Chen, K. S. 1983 Experimental study of free and mixed convective flow of air in a heated cavity. Final report to Sandia National Laboratories relating to experimental work performed for contract no. 20-1012. Also available as *Report no. FM-83-1, Department of Mechanical Engineering, University of California, Berkeley.*

Humphrey, J. A. C., Sherman, F. S., Le Quere, P. L. & Chen, K. S. 1980 Investigation of free-forced convection flow in cavity-type receivers. Mid-Term Report to Sandia National Laboratories. Also available as *Report no. FM-80-6, Department of Mechanical Engineering, University of California, Berkeley.*

Kraabel, J. S. 1983 An experimental investigation of the natural convection from a side-facing cubical cavity. *Proceedings of the ASME-JSME Thermal Engineering Joint Conference*, Honolulu, Hawaii, vol. 1 (ed. Y. Mori & W. J. Yang), pp. 299–306.

Le Quere, P. L., Humphrey, J. A. C. & Sherman, F. S. 1981 Numerical calculation of thermally-driven two-dimensional unsteady laminar flow in cavities of rectangular cross-section. *Num. Heat Transfer* **4**, 249–283.

Lloyd, J. R. & Sparrow, E. M. 1970 On the instability of natural convection flow on inclined plates. *J. Fluid Mech.* **42**, 465.

McLaughlin, D. K. & Tiederman, W. G. 1973 Biasing correction for individual realization of laser anemometer measurements in turbulent flows. *Physics Fluids* **16**, 1082–1088.

Mirenayat, H. 1981 Etude expérimentale de transfert de chaleur par convection naturelle dans une cavité isotherme ouverte. Ph.D. thesis, University of Poitiers, France.

Penot, F. 1981 Contribution a l'étude de la convection naturelle dans les espaces semi-confines. Ph.D. thesis, University of Poitiers, France.

Penot, F. 1982 Natural convection in isothermal open cavities. *Num. Heat Transfer* **5**, 421–437.

Pera, L. & Gebhart, B. 1973 On the stability of natural convection boundary layer flow over horizontal and slightly inclined surfaces. *Int. J. Heat Mass Transfer* **16**, 1147–1163.

Rotem, Z. & Claassen, L. 1969 Natural convection above unconfined horizontal surfaces. *J. Fluid Mech.* **39**, 173–192.

Sernas, V. & Kyriakides, I. 1982 Natural convection in an open cavity, *Proceedings of the Seventh International Heat Transfer Conference, Munich, Fed. Rep. of Germany*, vol. 2 (ed. U. Grigull, E. Hahne, K. Stephan & J. Straub), pp. 275–280.

Serrin, J. 1972 The swirling vortex. *Phil. Trans. R. Soc. Lond.* A **271**, 325–360.

PHILOSOPHICAL TRANSACTIONS OF THE ROYAL SOCIETY A MATHEMATICAL, PHYSICAL & ENGINEERING SCIENCES

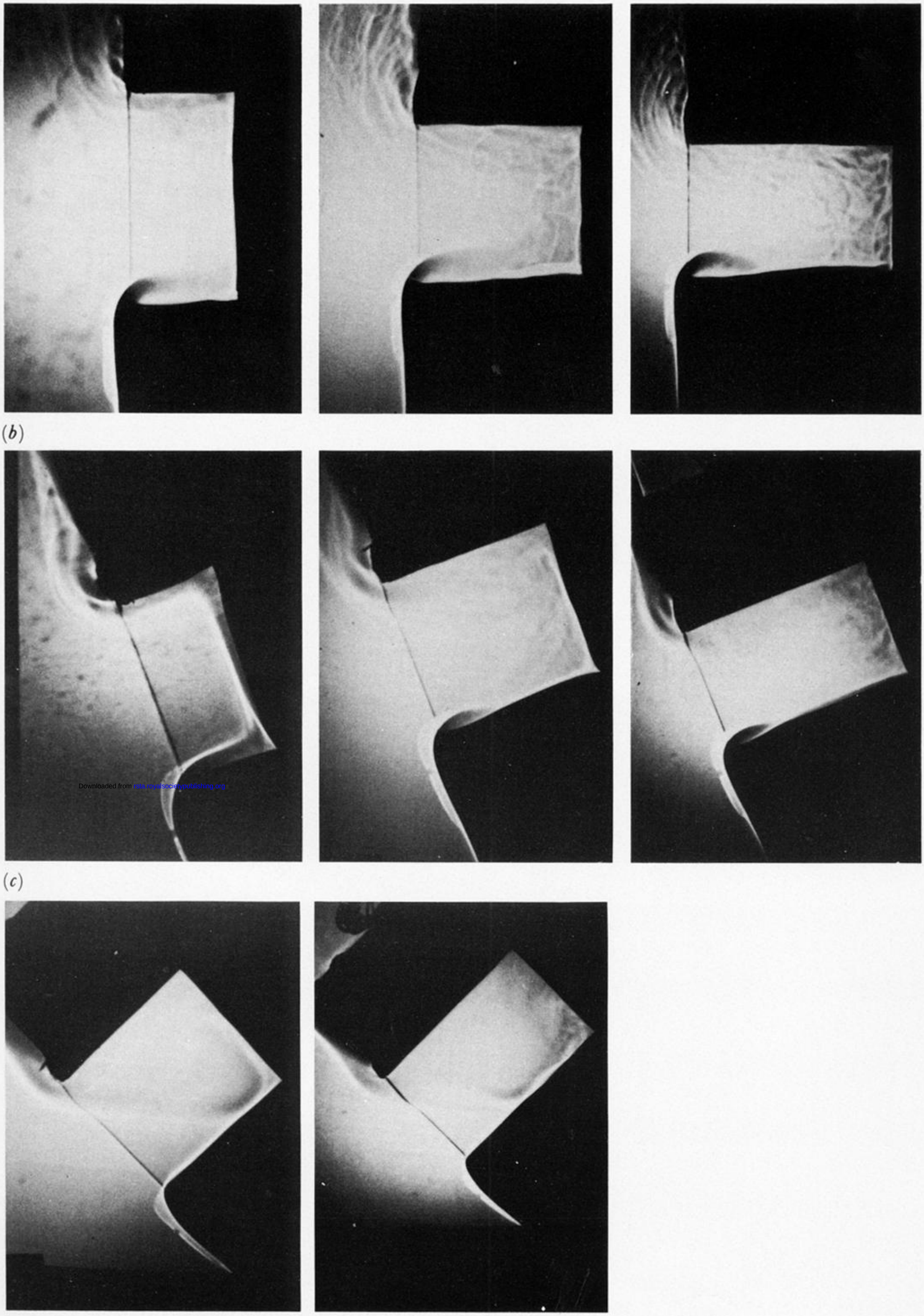

FIGURE 2. Shadowgraphs of the free-convection flow of air in rectangular cavities with $a/b = 0.5$, 1.0 and 1.46 (left to right) for three inclination angles of α: (*a*) 0°; (*b*) 20°; (*c*) 45°. Flow conditions: $\Delta T/T_\infty \approx 1.2$, $Gr \approx 4.2 \times 10^7$, $Pr \approx 0.7$. In all experiments the cavity aperture dimension, b, was the same. Unequal photographic reductions give the false impression that b varied.

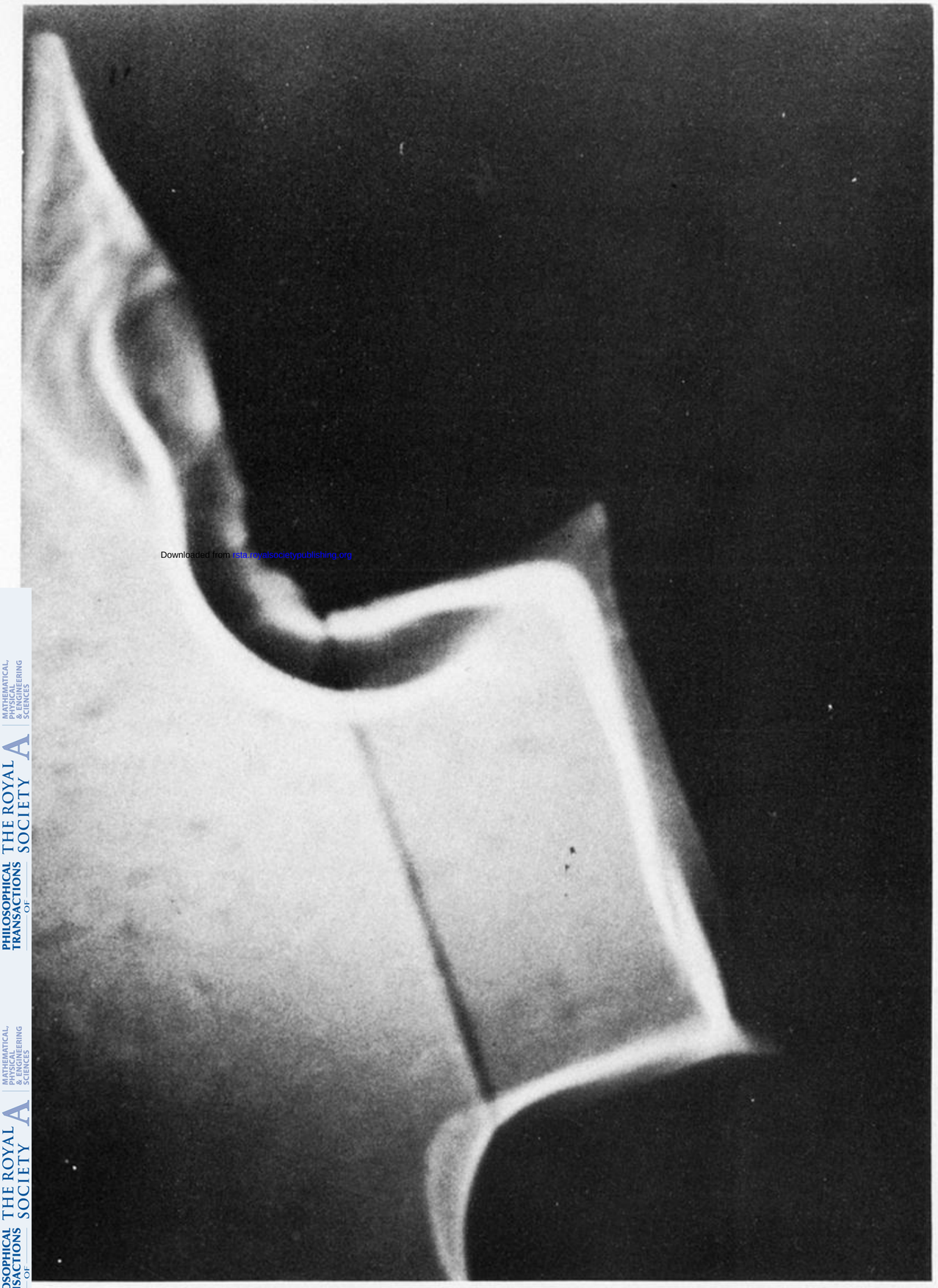

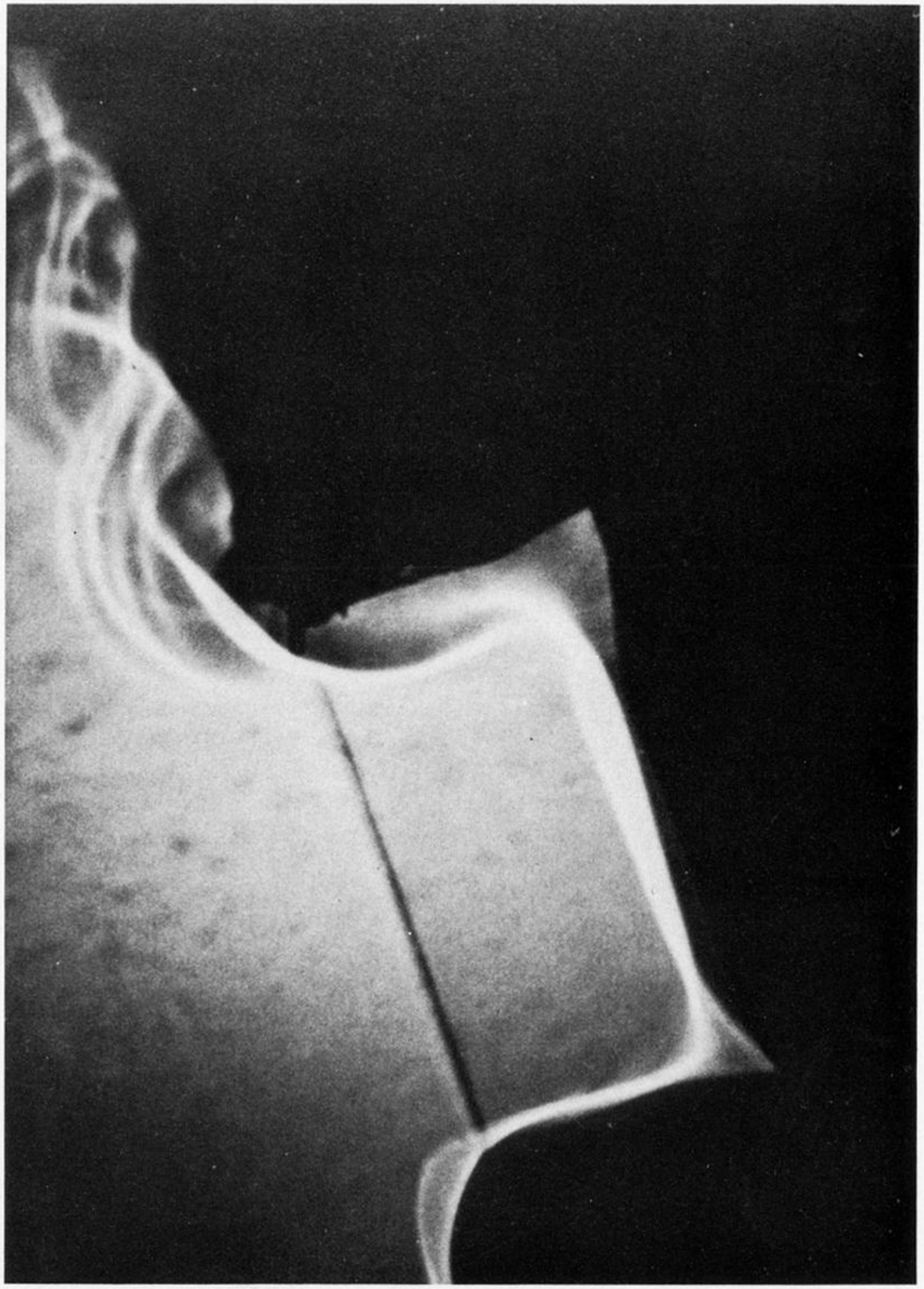

FIGURE 16. Large-scale, low-frequency organized cavity-flow oscillations frozen by stroboscopic pulsing of a point light source. Photographs are for different phases of a cycle.

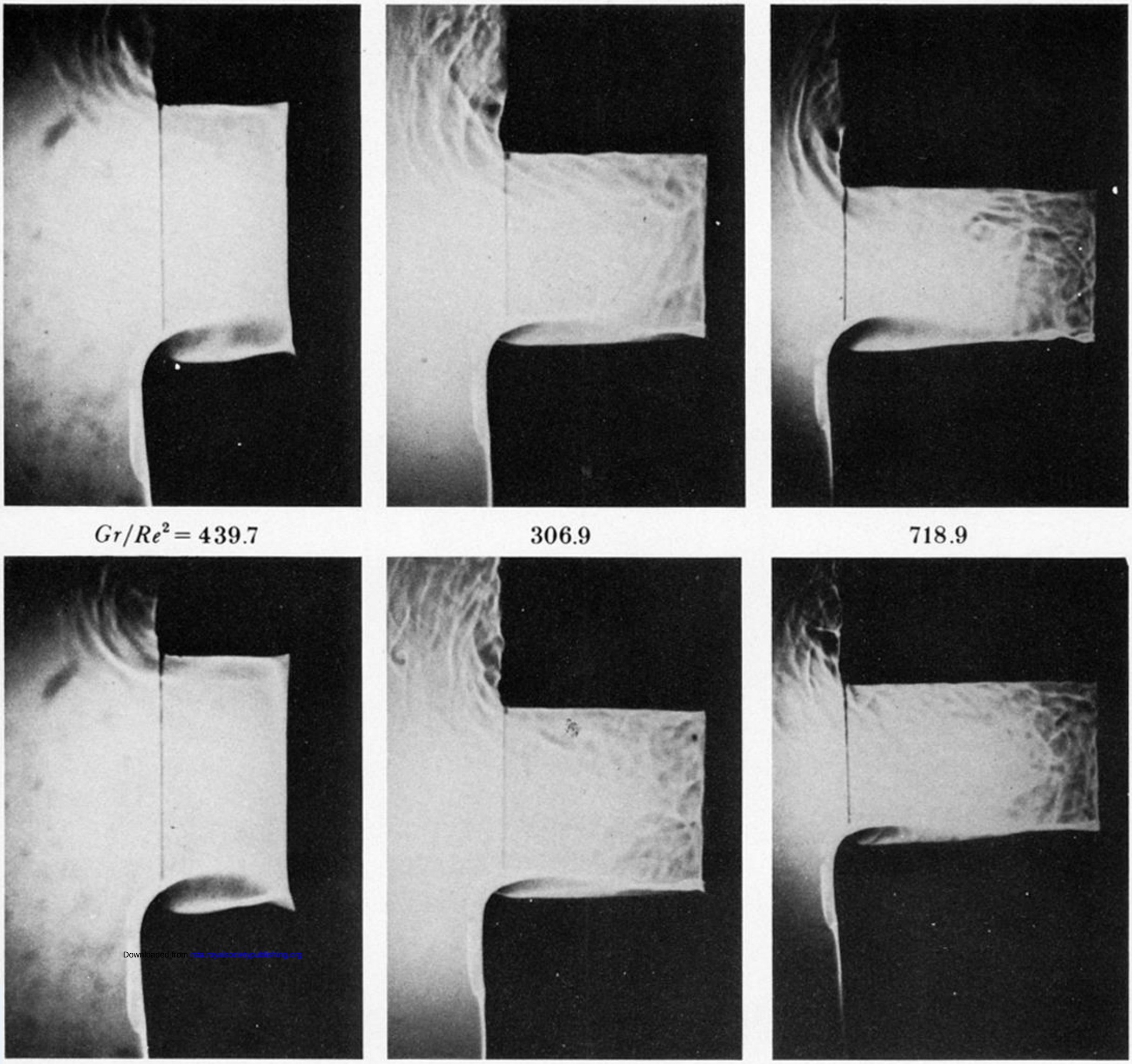

IGURE 17. Shadowgraphs of heated-cavity flows with $\alpha = 0°$ and (from left to right) $a/b = 0.5$, 1.0 and 1.46 for different values of Gr/Re^2: $Gr \approx 4.1 \times 10^7$, $\Delta T/T_\infty \approx 1.2$ (average values).

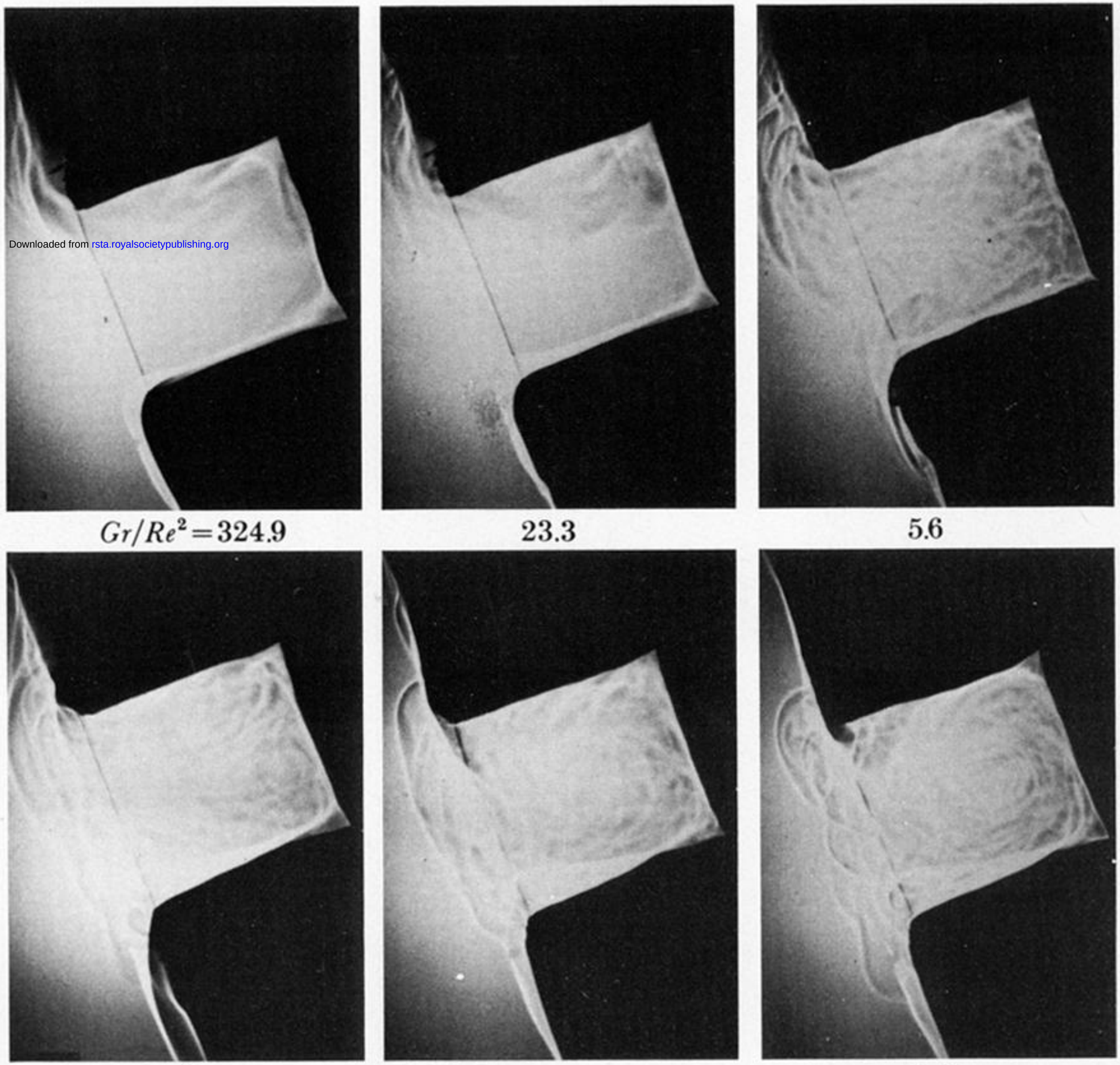

FIGURE 18. Shadowgraphs of heated-cavity flows with $a/b = 1.0$ and $\alpha = 20°$ for different values of Gr/Re^2: $Gr \approx 4.3 \times 10^7$, $\Delta T/T_\infty \approx 1.26$.

PHILOSOPHICAL TRANSACTIONS OF THE ROYAL SOCIETY A MATHEMATICAL, PHYSICAL & ENGINEERING SCIENCES

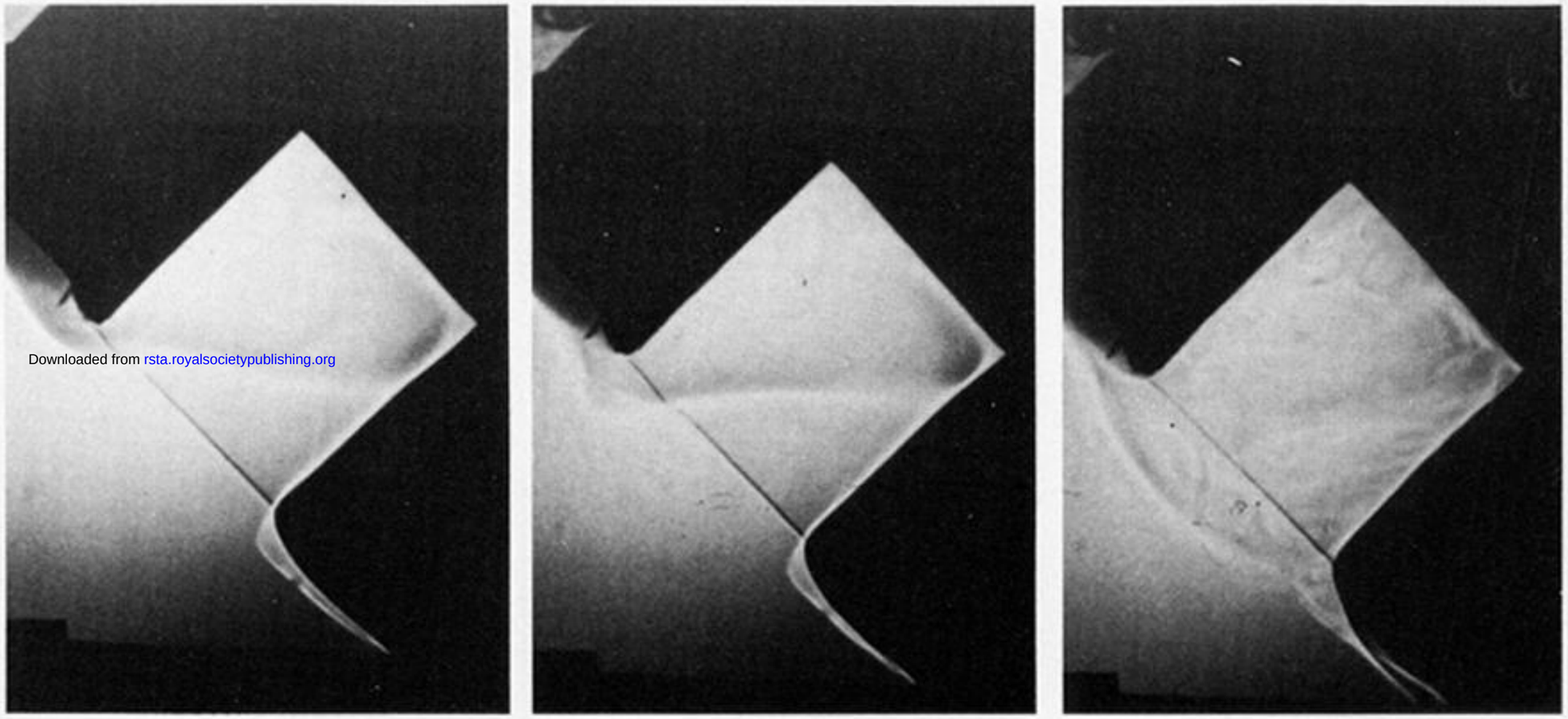

FIGURE 19. Shadowgraphs of heated-cavity flows with $a/b = 1.0$ and $\alpha = 45°$ for different values of Gr/Re^2: $Gr \approx 4.3 \times 10^7$, $\Delta T/T_\infty \approx 1.26$.

PHILOSOPHICAL TRANSACTIONS OF THE ROYAL SOCIETY A MATHEMATICAL, PHYSICAL & ENGINEERING SCIENCES